

Review

Advances in Cathodes for High-Performance Magnesium-Sulfur Batteries: A Critical Review

Ying Ying Yao ¹, Yang Zhan ¹, Xin Yu Sun ¹, Zhao Li ¹, Hao Xu ¹, Richard M. Laine ² and Jian Xin Zou ^{1,3,4,*}¹ National Engineering Research Center of Light Alloys Net Forming & State Key Laboratory of Metal Matrix Composites, Shanghai Jiao Tong University, Shanghai 200240, China² Department of Materials Science and Engineering, University of Michigan, Ann Arbor, MI 48109-2136, USA³ Shanghai Key Laboratory of Hydrogen Science & Center of Hydrogen Science, Shanghai Jiao Tong University, Shanghai 200240, China⁴ Shanghai Engineering Research Center of Mg Materials and Applications & School of Materials Science and Engineering, Shanghai Jiao Tong University, Shanghai 200240, China

* Correspondence: zoujx@sjtu.edu.cn

Abstract: Large-scale energy storage with high performance and at a reasonable cost are prerequisites for promoting clean energy utilization. With a high theoretical energy density of 1722 Wh·kg⁻², high element abundance (e.g., Mg of 23,000 ppm, S of 950 ppm on earth), and low theoretical cost, Mg-S batteries offer considerable potential as candidates for electrical energy storage. However, due to the intrinsic complex reaction chemistry of sulfur cathodes and metal anodes, such as slow diffusion of the divalent ion, the shuttle of soluble polysulfide, and irreversible deposition of Mg ions on metal electrodes, Mg-S batteries still need further optimization to meet requirements for practical applications. In addition to stabilizing metal anodes, developing a suitable sulfur cathode is desperately needed. This review summarizes recent research progress in sulfur cathodes, interlayers, and non-nucleophilic electrolytes, highlighting the main challenges and corresponding strategies for electrode material designs. Notably, we emphasize a fundamental understanding of the structure-composition relationship. Furthermore, state-of-the-art characterization techniques are described that help reveal the pertinent electrochemical mechanisms whereby Mg-S cells function. Finally, possible research directions are discussed.

Keywords: magnesium sulfur batteries; sulfur-based cathodes; Mg polysulfides; interlayer modification; functional separator



Citation: Yao, Y.Y.; Zhan, Y.; Sun, X.Y.; Li, Z.; Xu, H.; Laine, R.M.; Zou, J.X. Advances in Cathodes for High-Performance Magnesium-Sulfur Batteries: A Critical Review. *Batteries* **2023**, *9*, 203. <https://doi.org/10.3390/batteries9040203>

Academic Editor: Carolina Rosero-Navarro

Received: 14 February 2023

Revised: 22 March 2023

Accepted: 27 March 2023

Published: 29 March 2023



Copyright: © 2023 by the authors. Licensee MDPI, Basel, Switzerland. This article is an open access article distributed under the terms and conditions of the Creative Commons Attribution (CC BY) license (<https://creativecommons.org/licenses/by/4.0/>).

1. Introduction

To achieve word-wide carbon-neutrality, tremendous attempts have been made to reduce carbon emissions, putting great pressure on developing green energy technology [1]. However, green energy technologies, such as solar, wind, and tidal, are limited by geography or time uncertainty. Because of this, developing large-scale energy storage conversion systems are urgently required. Although lithium-ion batteries (LIBs) are widely used, they still suffer from critical defects, including limited reserves, high cost, and potential security liability [2,3]. Consequently, beyond Li⁺, e.g., Na⁺, K⁺, Mg²⁺, Zn²⁺, and Al³⁺ batteries remain appealing [4,5]. Among them, rechargeable magnesium-ion batteries (RMBs) have aroused wide interest, ascribed to Mg metal's high theoretical volume specific capacity of 3833 mAh·cm⁻³, which is close to twice that of lithium (2046 mAh·cm⁻³) and nearly five times that of graphite (800 mAh·cm⁻³). Although magnesium's standard electrode potential (Mg²⁺/Mg, -2.36 V vs. SHE) is lower than lithium (Li⁺/Li, -3.05 V vs. SHE), it is significantly higher than aluminum and zinc (Al³⁺/Al, -1.66 V vs. SHE; Zn²⁺/Zn, -0.76 V vs. SHE) [5,6].

Magnesium primary batteries were first commercialized in 1943 (Figure 1), offering a voltage plateau of 1.6 V, and are widely used in military and aerospace backup power sup-

plies [7]. Gregory and co-workers at Dow Inc. initiated research on RMB electrolytes with high Coulombic efficiencies beginning in 1990 [8]. In early 2000, Aurbach and colleagues [9] made use of Chevrel phase Mo_6S_8 in RMBs, achieving more than 2000 cycles, signifying a breakthrough for RMB technology. A second breakthrough came with the discovery of all-phenyl-complex (APC) electrolyte by Aurbach and co-workers [10]. In 2011, Kim and Muldoon et al. first proposed a proof-of-concept Mg-S battery with a non-nucleophilic electrolyte of $\text{MgCl}_2(\text{HMDS})\text{-AlCl}_3$, with a high discharge capacity of $1200 \text{ mAh}\cdot\text{g}^{-1}$ and $2484 \text{ mAh}\cdot\text{cm}^{-3}$ [11]. Since then, Mg-S battery research has drawn increasing interest because of the natural earth abundance of the raw materials (e.g., Mg of 23,000 ppm, S of 953 ppm), $1680 \text{ Wh}\cdot\text{kg}^{-1}$ and $3220 \text{ Wh}\cdot\text{L}^{-1}$ theoretical energy density, a suitable potential window in ether-based electrolytes, and improved safety from dendrite-free deposition behavior [12–15].

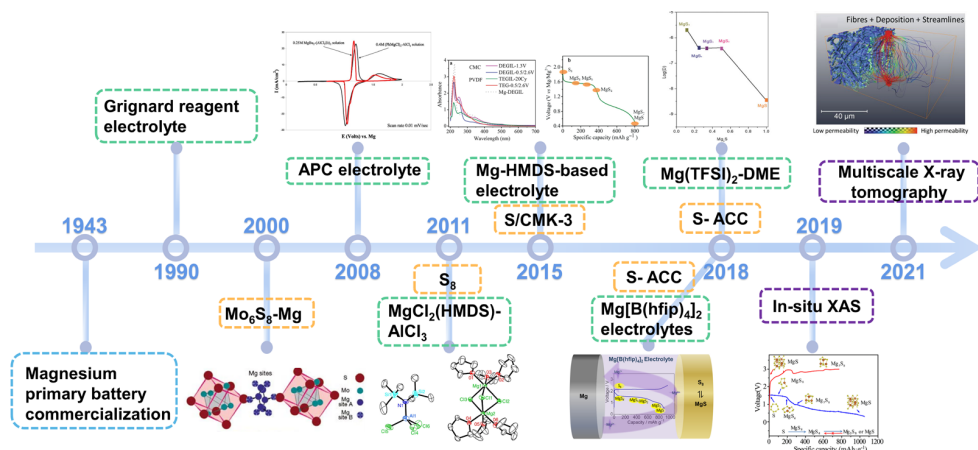


Figure 1. The history of RMB development beginning in 1943 in terms of electrolyte (green), cathode (orange), and characterization techniques (purple). Grignard reagent electrolytes [8]. Mo_6S_8 as RMB cathode materials [9]. The invention of APC electrolyte [10]. The first proof-of-concept Mg-S battery using $\text{MgCl}_2(\text{HMDS})\text{-AlCl}_3$ electrolyte [11]. The first application of ionic liquids as the electrolyte solvents and S/CMK-3 as the cathode [16]. Investigation of $\text{Mg}[\text{B}(\text{hfip})_4]_2$ electrolyte [17]. The first use of S/ACC active material [18]. In situ XAS [19] and multiscale X-ray tomography [20] applied to investigate the electrochemical conversion in Mg-S batteries.

Despite its promise, multiple scientific problems need resolution. For example, the rapid and facile formation of MgO severely passivates Mg metal anode surfaces, and Mg^{2+} exhibits high polarization greatly impeding diffusion in cathode lattices. Gao et al. [18] used X-ray photoelectron spectroscopy (XPS) analysis and found that the discharge path in Mg-S batteries is akin to Li-S batteries, for which multiple processes $\text{S}_8 \rightarrow \text{MgS}_8 \rightarrow \text{MgS}_4 \rightarrow \text{MgS}_2 \rightarrow \text{MgS}$ occur, indicating that Mg-S batteries must be designed to overcome polysulfide shuttling. In addition, as an electrophilic cathode, sulfur must be matched with a non-nucleophilic electrolyte to avoid side reactions. However, regarding Mg-S battery technology itself, cathode materials' development is still in its infancy. There is a critical need to understand and improve the structure and compositions of cathode materials to enhance storage capacity, rate capability, and cycling performance.

In this overview, we sum up research progress in sulfur cathodes, interlayers, and non-nucleophilic electrolytes, highlighting current major challenges that must be resolved to realize commercially viable Mg-S batteries, as well as electrode material design principles. Notably, our focus is on presenting a basic understanding of structure-composition relationships. In addition, state-of-the-art characterization techniques are described to help unveil electrochemical behavior in Mg-S batteries. Finally, possible research directions toward practical applications are discussed.

2. Reaction Mechanisms and Challenges in Mg-S Batteries

2.1. Reaction Mechanisms in Mg-S Batteries

Although Mg-S batteries were first proposed in 2011, there remain multiple electrochemical reactions and failure mechanisms to be clarified [21,22]. Schemes I-III present sulfur reduction mechanisms extant during the discharge process. Figure 2 illustrates the process whereby elemental sulfur gradually generates long-chain polysulfides (LCSs) that are then reduced to short-chain sulfides (SCSs) or MgS.

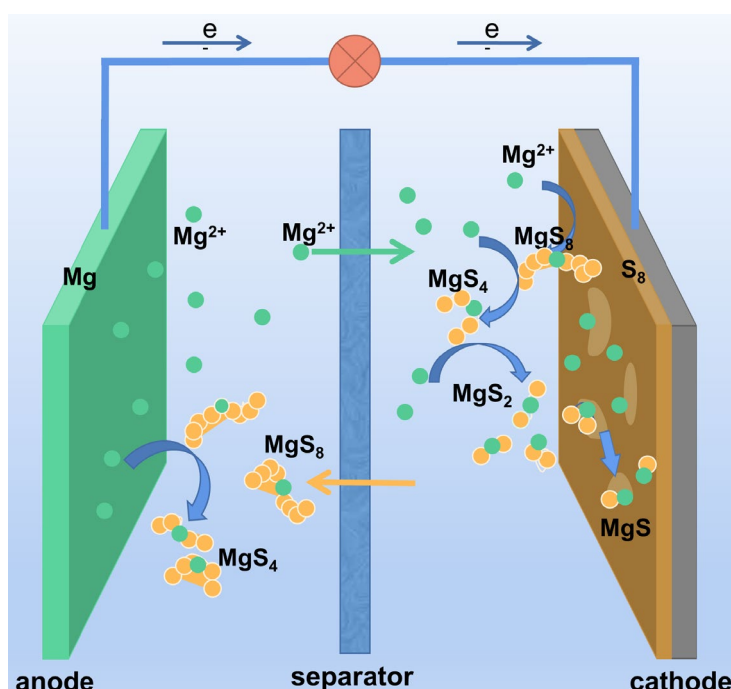
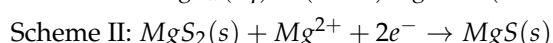
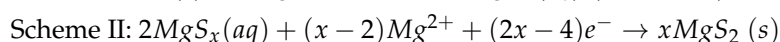
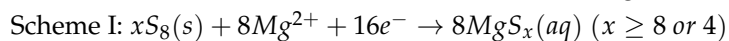


Figure 2. Illustration discharge reaction mechanism for Mg–S batteries.

As mentioned above, Gao et al. [18] found by XPS that sulfur first forms LCSs at 2.4–1.5 V, and then SCSs at 1.5 V, and finally MgS at 1.5–0.5 V in $Mg(TFSI)_2$ -DME electrolyte (Figure 3a). According to the kinetic factor obtained from CV curve fitting and ab initio molecular dynamics (AIMD) simulation, Schemes I and II are mixing-controlled reactions, while Scheme III is a diffusion-controlled reaction. As MgS exhibits a strong tendency to crystallize and MgS_x ($x = 2–8$) tends to remain amorphous, Mg^{2+} diffusion becomes difficult when MgS is generated at the interface and the final product has a Mg concentration gradient from interface to depth. The reaction mechanisms for Mg-S batteries with S/CMK-3 cathodes and Mg-HMDS-based (glymes and additional ionic liquid as solvents) electrolyte were also investigated by Zhao-Karger and co-workers (Figure 3b,c) [16]. During discharge, S_8 first forms MgS_4 at 1.6 V offering a capacity of $\sim 400\text{ mAh}\cdot\text{g}^{-1}$. Thereafter, liquid-solid interfacial reduction occurs generating MgS_2 with a theoretical capacity of $840\text{ mAh}\cdot\text{g}^{-1}$, followed by reduction to MgS. This last process suffers from high dynamic barriers and polarization. Roughly the same conclusions can be reached for different electrolytes.

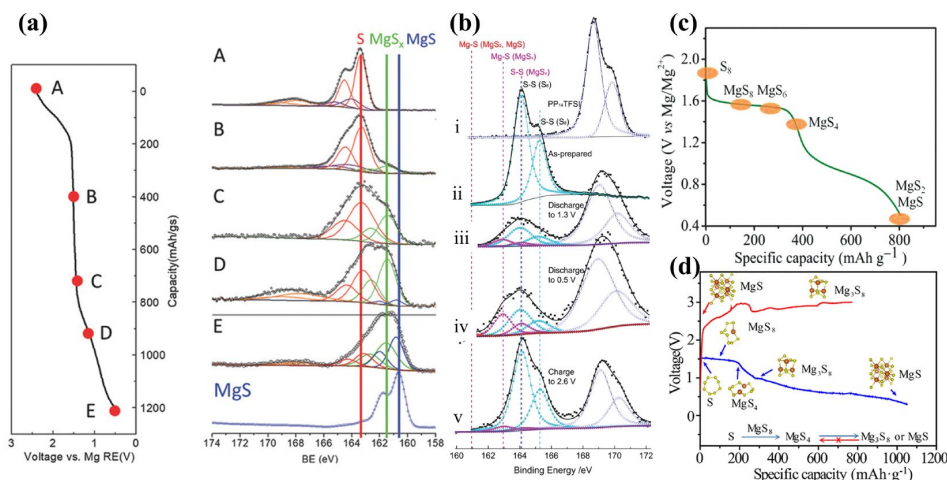


Figure 3. (a) XPS S 2p spectra of S/ACC cathode (S/C ratio = 0.11) at different states [18]. (b) XPS of S/CMK400PEG cathode and Mg(HMDS)₂ base electrolyte with ionic liquid PP14TFSI additives: (i) PP14TFSI, (ii) S/CMK400PEG, (iii) discharged to 1.3 V, (iv) discharged to 0.5 V, and (v) charged to 2.6 V, and (c) corresponding proposed mechanisms of discharge process [16]. (d) Charge–discharge curves and proposed mechanisms in Mg(HMDS)₂–based electrolyte [19].

Furthermore, researchers have used various *in situ* techniques to clarify Mg-S cell reaction mechanisms [19,23]. Dominko et al. used *in situ* XANES and RIXS to study Mg-S battery mechanisms, finding that S₈ converts to polysulfides at a high voltage plateau and is then reduced to solid MgS. They also used NMR to characterize the discharge products. Mg is tetrahedrally coordinated in electrodeposited MgS, similar to wurtzite, while Mg in chemically synthesized MgS is octahedrally coordinated. Xu and co-workers [19] used density functional theory (DFT) calculations and *in situ* synchrotron X-ray absorption spectroscopy (XAS) to confirm that Mg₃S₈ produced in stage II is insoluble in the electrolyte; a consequence of an overpotential during cycling (Figure 3d). Moreover, the discharge products Mg₃S₈ and MgS have poor electrochemical activity and are difficult to oxidize to high-order polysulfides or sulfur, which leads to rapid capacity decay after the first discharge, reducing the cycle life. Coincidentally, Bhardwaj et al. [24] applied operando Raman spectroscopy to confirm the existence of higher-order Mg-polysulfides at high-voltage plateaus.

In addition, the dissolution and shuttling of S₈ and polysulfides in electrolytes is also a critical problem [16,25,26]. Yellow discoloration of separators is often found in Mg-S batteries after a few cycles, indicating dissolved polysulfides [11]. Haecker and co-workers [23] used operando UV-Vis spectroscopy to determine the self-discharge behaviors under state of charge. After an OCV rest, severe self-discharge occurs, which can be divided into three stages: First, sulfur dissolves and is reduced to S₆⁻² and S₄⁻² on the Mg anode. Then, the S₈ concentration in the electrolyte reaches equilibrium and the concentration of S₆⁻² and S₄⁻² increase steadily. Finally, the concentrations of S₈, S₆⁻², and S₄⁻² reach equilibrium. About 0.6% sulfur in the form of MgS_x was found on Mg foils after 50 cycles by ex situ XPS [27]. Coincidentally, Kimberly A et al. [25] employed a quasi-reference electrode of Ag₂S to investigate the reaction between Mg metal and polysulfides, discovering severe reduction overpotential on the Mg anode surface (Figure 4a,b). Based on the shuttling of polysulfides, Mg is passivated in early cycles (Figure 4c). In another report, Zhao-Karger et al. [17] used X-ray energy dispersion spectroscopy (EDS) to analyze the elemental composition of the Mg anode after the 2nd and 18th cycles in sulfur-impregnated activated-carbon cloth (ACCS)-Mg cells, Figure 4d. Elemental sulfur was not detected on the Mg surface after the 2nd cycle, but was evident on the 18th cycle, indicating formation of MgS_x or S films. However, there are no unifying conclusions on the failure mechanisms of Mg-S batteries. Hence, systematic research on the reaction mechanisms is still important as a prerequisite to identifying strategies for ameliorating known problems.

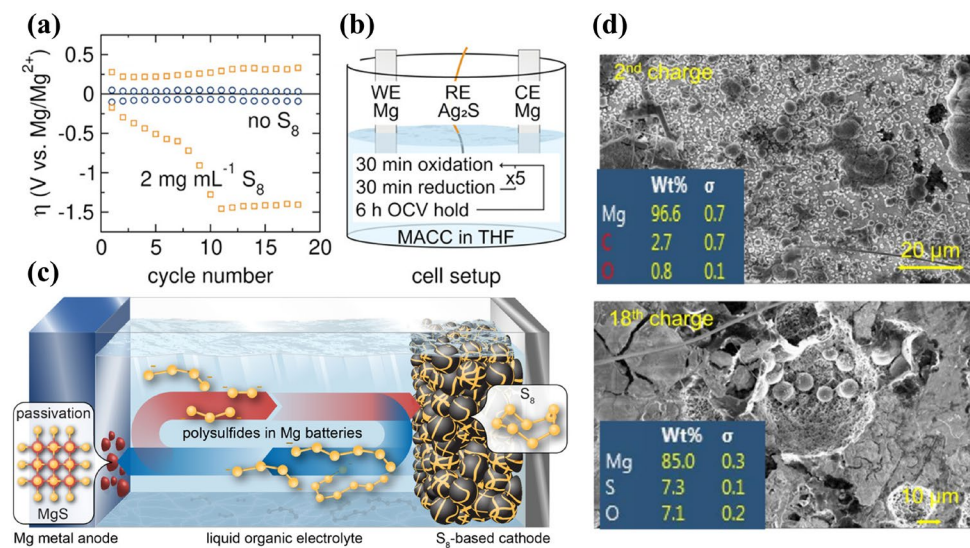


Figure 4. (a) Overpotential tests in Mg Symmetrical cells with and without $2 \text{ mg}\cdot\text{mL}^{-1} \text{ S}_8$; (b) Schematic diagram of the three-electrode test; (c) Self-discharge and anode passivation mechanisms for Mg–S batteries [25]. (d) Mg foil EDS in $\text{Mg}[\text{B}(\text{hfip})_4]_2$ electrolyte after different cycle numbers [17].

2.2. Challenges in Cathode Materials

Dan-Thien and co-workers summarized failure mechanisms for Mg–S batteries, as shown in Figure 5 [28]. To address these weaknesses, researchers have proposed various solutions, such as the improved design of electrolytes [29,30], exploration of solid-state cells [31], synthesis of artificial anode SEIs [32], and the introduction of improved designs for cathode compositions and structures. Here, we present a review of the main challenges and strategies for the cathode side.

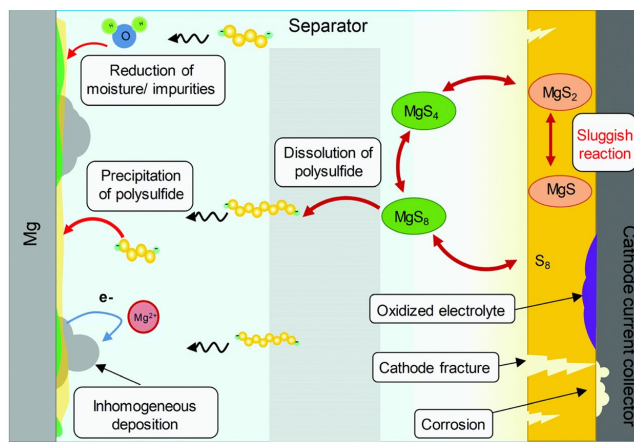


Figure 5. The general failure mechanism for Mg–S batteries [28].

(1) Improving the conductivity of electrode materials. Sulfur with an electric conductivity of $5 \times 10^{-30} \text{ S}\cdot\text{cm}^{-1}$ at room temperature functions as an electrical insulator, leading to severe ohmic polarization in Mg–S batteries. Therefore, compounding with highly conductive materials is a widely used strategy. For instance, graphene, carbon nanotubes (CNTs), MXenes, active carbon cloth (ACC) [18,33–36], and other materials [24,37,38] have been explored extensively.

(2) Prohibiting the effects of sulfur and polysulfide shuttling. As previously mentioned, the shuttling of sulfur and polysulfides in electrolytes often causes self-discharge, low Coulombic efficiency, and anode passivation, leading eventually to battery failures. Self-discharge has been verified systematically in different electrolytes, such as $\text{Mg}[\text{B}(\text{hfip})_4]_2$ /

DME, MgFPB/DEG, and Mg(HMDS)₂-AlCl₃/THF [26,39–41]. SCSs are more likely to generate MgS on the Mg anode compared to LCSs, while MgS is an electrochemically inert material with a low Mg²⁺ diffusion rate, which partially passivates Mg surfaces [25].

Various types of sulfur hosts have been used to mitigate shuttling effects, of which physical confinement and chemisorption are well-known methods. Meanwhile, organic sulfur copolymers have been introduced to anchor sulfur by covalent bonding [42,43]. Recently, coatings or interlayers have been used between cathode/electrolyte to prohibit S₈ and magnesium polysulfide transport, thereby eliminating any reaction of the anode with sulfur species [44–46].

(3) Mitigating the formation of stable compounds with low-formation energy. Mg-S batteries typically show severe capacity degradation from the second cycle, accompanied by high charge/discharge polarization. The discharge products in Mg(HMDS)₂-based electrolytes were thoroughly investigated by Xu et al. [19] using *in situ* XAS measurement (Figure 3d). The discharge products Mg₃S₈ and MgS are nearly inert and do not reverse to higher-order magnesium polysulfides and S₈, leading to rapid capacity degradation in subsequent cycles. Nakayama and co-workers [47] found that metastable zinc blende MgS is electrochemically active, while rock salt MgS is electrochemically inert.

(4) Enhancing cathodic mass transfer and reaction kinetics. High charge density is the source of slow Mg²⁺ diffusion in solids, more than twice that of Li⁺, leading to poor kinetics for Mg-S batteries. Lu and co-workers [48] reported that Mg-S batteries have lower concentrations of polysulfides during charge and discharge compared to Li-S batteries as determined by operando UV-Vis spectroscopy. Through three-electrode electrochemical characterizations, a stable low solubility S₂²⁻ forms at the very beginning of discharge, which leads to the high overpotential at the cathode, and accounts for more than 50% of the cell overpotential. Thus, the first discharge capacity was successfully increased from 650 mAh·g⁻¹ to 1500 mAh·g⁻¹ by using dimethyl sulfoxide (DMSO) as a solvent. According to the above, increasing the solubility of MgS_x could improve polysulfide dynamic performances and active material utilization rate. Furthermore, the application of lithium salt additives is also widely used to lower the kinetic barriers of Mg-S cells [49].

Eventually, to realize the commercialization of Mg-S batteries, researchers must focus on low-priced materials, lower electrolyte solution/sulfur (E/S) ratios and carbon/sulfur (C/S) ratios, and prolong the battery cycle life.

3. Research Progresses on Sulfur Cathodes

To alleviate the dissolution and shuttle effects of polysulfides, various sulfur hosts have been proposed; classified as physical adsorption, chemisorption, and hybrid adsorption [50]. In the following, we also discuss interlayers between the cathode interface, electrolyte, and functional separators.

3.1. Physical Adsorption Cathode

Mg-S cells suffer from issues, especially polysulfide dissolution and shuttling, the insulating behavior of S₈, and critical electrode volume changes. In principle, physically trapped sulfur compounds with high electronic conductivity and chemical durability can improve sulfur utilization, mitigate polysulfide migration and retard the volume expansion of cathode active materials. Widely explored physically adsorbed sulfur hosts including activated-carbon cloth (ACC) [18,33–36] and porous carbon materials [24,37,38].

Sulfur-impregnated ACC (S/ACC) as a promising method for creating physically trapped “sulfur” for Li-S cells was first explored by Aurbach et al. [51]. It permits binder-free, exceptionally conductive three-dimensional structures, and superior specific surface areas (SSAs), which can decrease the escape of polysulfides allowing high sulfur utilization. Sulfur access to carbon fiber pores in ACC is achieved by melt-diffusion at 155 °C. The structure of a S/ACC composite cathode is shown in Figure 6a. Gao and co-workers [18] applied sulfur-impregnated ACC to investigate sulfur chemistry in Mg-S batteries with Mg(TFSI)₂-DME electrolyte, which shows that S₈ reacts stepwise, as illus-

trated in Figure 6b–d. Figure 6b,c further illustrate Figure 6b. The different colored arrows in Figure 6b correspond to different ion and electron transport pathways, and Figure 6c shows a gradual decrease in x in MgS_x ($1 \leq x \leq 8$) as yellow shifts to brown, where brown indicates the formation of MgS . This also indicates the presence of a Mg concentration gradient in the final product from the electrode surface to depth. Moreover, a ~70% capacity retention cycling stability was found after 110 cycles through a combination of highly concentrated 1 M $\text{MgTFSI}_2/\text{MgCl}_2/\text{DME}$ electrolyte and sulfur-impregnated ACC (Figure 6e) [35]. However, this improved electrochemical performance was achieved on the basis of ultra-low S:C ratios of 0.11, unfortunately not yet useful for practical applications. Muthuraj [36] used magnesium-polysulfide (MgS_x) and polyaniline-coated carbon cloth (CC@PANI) to form self-supporting cathodes. First, a PANI layer was deposited on the ACC by in situ polymerization, and then the CC@PANI@ MgS_x cathode was synthesized by dropwise addition of MgS_x solution (Figure 7a). CC@PANI serves as both a chemisorption and physical adsorption material. CC@PANI@ MgS_x cathodes show a discharge capacity of $514 \text{ mAh} \cdot \text{g}^{-1}$ and are stable for more than 20 cycles. Currently, the S/ACC sulfur loading is usually below $2 \text{ mg} \cdot \text{cm}^{-2}$, resulting in ultra-low S:C ratios.

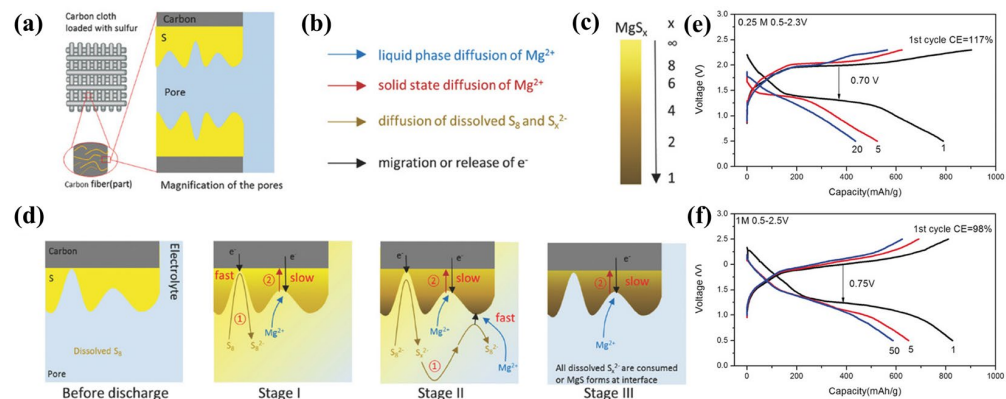


Figure 6. (a) Structure of the S/ACC composite cathode. (b–d) The proposed sulfur reduction mechanism. ① Surface magnesiation. ② Bulk magnesition. [18]. (e) The S/ACC electrochemical performance in various concentrations of $\text{MgTFSI}_2\text{--MgCl}_2/\text{DME}$ electrolytes [35].

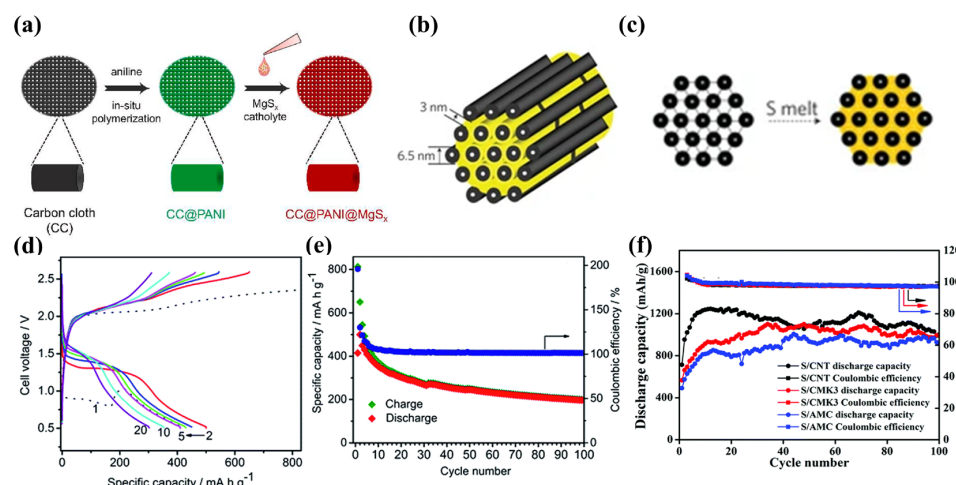


Figure 7. (a) Diagram of synthesis of CC@PANI@ MgS_x [36]. (b) CMK-3 structure schematic. (c) Preparation schematic diagram of S/CMK-3 [52]. (d,e) The S/CMK-3 electrochemical performance in $\text{Mg}[\text{B}(\text{hfip})_4]_2$ electrolyte. (f) S/AMC, S/CNT, and S/CMK-3 cycling performance in 0.5 M OMBB electrolyte with Cu current collector at $160 \text{ mA} \cdot \text{g}^{-1}$ [53].

CMK-3, a highly ordered mesoporous carbon, with SSAs up to $2500 \text{ m}^2 \cdot \text{g}^{-1}$ and pore volumes up to $2.25 \text{ cm}^3 \cdot \text{g}^{-1}$, can be considered to offer significant potential as a physical

absorption S host (Figure 7b) [16,52,54,55]. CMK-3 is first oxidatively carboxylated in HNO_3 solution at 80 °C, then melt-diffused with S_8 at 160 °C for 12 h (Figure 7c). S_8 fills the 3 nm pores of CMK-3 [52]. Zhao-Karger and coworkers used S/CMK-3 cathodes and the non-nucleophilic electrolyte of $\text{Mg}[\text{B}(\text{hfip})_4]_2/\text{DEG-TEG}$ in Mg-S cells, successfully demonstrating an initial discharge capacity of almost 400 $\text{mAh}\cdot\text{g}^{-1}$ and cycling performance of 200 $\text{mAh}\cdot\text{g}^{-1}$ after 100 cycles at 167 $\text{mA}\cdot\text{cm}^{-2}$ (Figure 7d,e) [55].

Carbon S/nanofiber [56] and S/ketjen black [41] physisorbed hosts have also been prepared by melt-diffusion, showing specific capacities of 920 $\text{mAh}\cdot\text{g}^{-1}$ and 770 $\text{mAh}\cdot\text{g}^{-1}$ respectively. Du and colleagues [53] compared the performances of S/amorphous mesoporous carbon (S/AMC), S/CMK-3, and S/CNTs in Mg-S batteries, all of which showed excellent cycling performance with copper collectors, with discharge-specific capacities higher than 800 $\text{mAh}\cdot\text{g}^{-1}$ after 100 cycles (Figure 7f). However, capacity decay was detected for most carbon hosts after 20 cycles without Cu current collectors or lithium-salt additives.

Two-dimensional transition metal compounds (MXenes) are attracting increasing attention for their high electrical conductivity, rich surface functionality, and unique two-dimensional morphology, especially in energy storage devices [57]. Kaland and coworkers [38] first proposed $\text{Ti}_3\text{C}_2\text{T}_x$ MXene as a free-standing material for Mg-S batteries. The cells achieved a specific capacity of 530 $\text{mAh}\cdot\text{g}^{-1}$ using an MXene interlayer (Figure 8a), and exhibited stable cycling with retention of >400 $\text{mAh}\cdot\text{g}^{-1}$ after 10 cycles, while the cells with no interlayer attained only 200 $\text{mAh}\cdot\text{g}^{-1}$ (Figure 8b). Xu [58] and Zhao [59] also prepared MXene with metal oxides/sulfide as a S host, which permits Mg^{2+} diffusion and transfer. S/ Co_3S_4 @MXene [59] with 75 wt.% sulfur loading and S/CoO@MXene [58] with 60 wt.% S loading exhibits high specific capacities of 1220 $\text{mAh}\cdot\text{g}^{-1}$ and 1500 $\text{mAh}\cdot\text{g}^{-1}$, respectively.

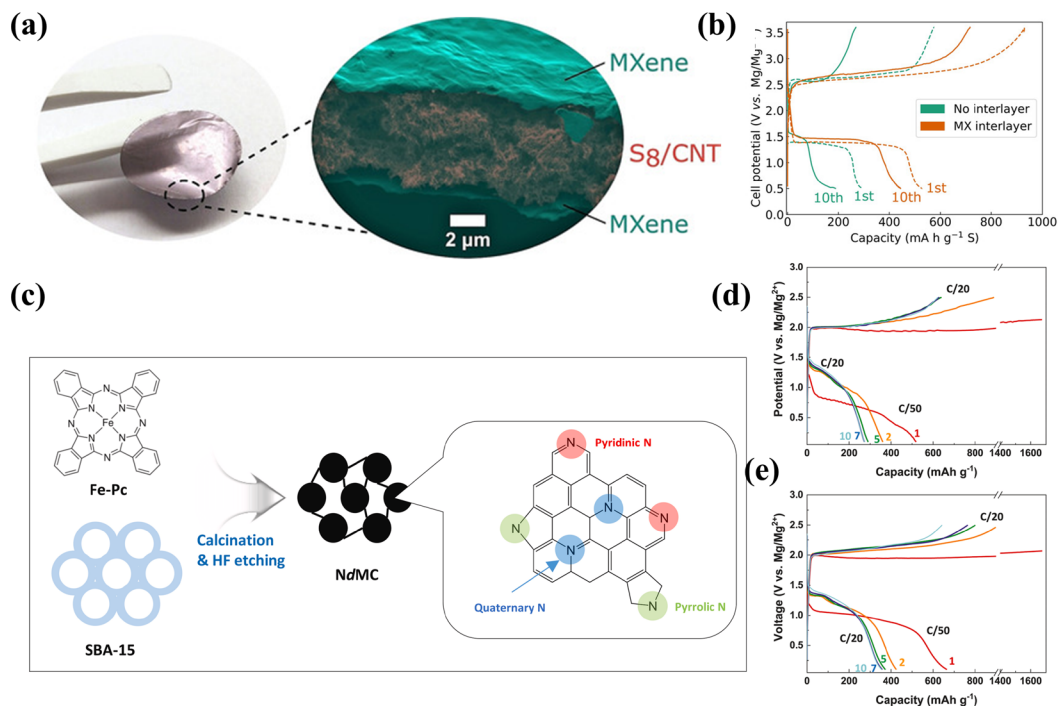


Figure 8. (a) Structural diagram of $\text{Ti}_3\text{C}_2\text{T}_x$ MXene as free-standing cathode, and the corresponding (b) charge–discharge curves in $\text{Mg}[\text{B}(\text{hfip})_4]_2$ electrolyte [38]. (c) NdMC synthesis schematic. Charge–discharge curves of (d) S/CMK–3 cathode and (e) S/NdMC cathode [37].

3.2. Chemisorbed Cathode

Strengthening stable chemical bonds with sulfur via heteroatoms in the host structure is an effective strategy to enhance sulfur loading and reduce polysulfide solubilization [60]. Lee et al. [37] demonstrated that N-doped mesoporous carbon (NdMC, Figure 8c) can serve as promising catalytic hosts that suppress magnesium polysulfide dissolution in

electrolytes. The synergistic effect ascribed to nitrogen in NdMC comes from a strong chemical affinity for Mg polysulfides while also offering an electron-deficient structure to accelerate electron transfer between critical sites. As a result, the plateau potential of S_8 @NdMCs is 0.2 V or higher than that of S_8 @CMK-3 (Figure 8d,e). Pyridinic-N in S_8 @NdMCs also effectively promotes S_6^{2-} diffusion to generate MgS as determined by UV-Vis studies.

Metal-organic frameworks (MOFs) with ultra-high SSAs, for instance, UN-110, show an SSA of $7000\text{ m}^2\cdot\text{g}^{-1}$; and diverse topologies, have been shown to capture polysulfides by appropriate channel structures and strong chemical interactions [45,49,61,62]. Li's group [49] used a MOF-derived carbon matrix as an S host with a sulfur loading of 47 wt.%, synthesized by thermolysis of ZIF-67 under an inert atmosphere, followed by acid leaching with H_2SO_4 to degrade active metallic particles, followed by a thermal process to diffuse S_8 into the pores or interstices of N- and Co-doped carbon (ZIF-C) (Figure 9a). The potential catalysis by Co species and N-doped carbon in ZIF-C coupled with an rGO-coated separator exhibited a specific capacity of $>900\text{ mAh}\cdot\text{g}^{-1}$ in Mg-S batteries, maintaining a capacity of $450\text{ mAh}\cdot\text{g}^{-1}$ after 250 cycles at 0.1 C with highly concentrated Li-salt additives. Complicated syntheses result in high manufacturing costs in addition to the charge-discharge profiles in Figure 9b,c, high concentrations of Li-salts play a pivotal role in ensuring the good kinetic performance of these Mg-S cells, with further increases in costs.

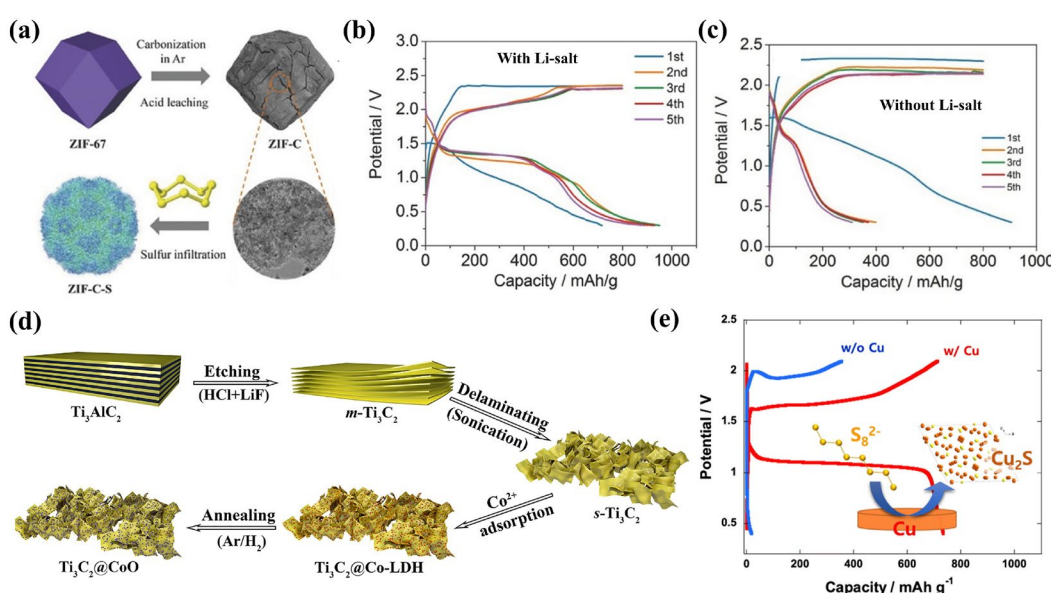


Figure 9. (a) S/ZIF-C synthesis method. (b) The discharge–charge profiles (b) with added LiTFSI and (c) without added LiTFSI in $\text{Mg}(\text{HMDS})_2$ -base electrolyte [49]. (d) Ti_3C_2 and $\text{Ti}_3\text{C}_2@\text{CoO}$ synthesis methods [58]. (e) Comparison of charge–discharge profiles for copper (red) and aluminum (blue) current collectors [63].

In parallel with metal elements [64] and nitrogen-doped carbon [37], metal oxides [58], sulfides [44,59,65], phosphides [45], and nitrides [23] have also been shown to be effective adsorbents for magnesium polysulfides. Xu and coworkers [58] demonstrated the strong adsorption of polysulfides on CoO by UV-Vis spectroscopy, XPS, and DFT calculations, and synthesized MXene@CoO lamellar structures that also facilitate the transport of Mg species (Figure 9d). $\text{S}/\text{Ti}_3\text{C}_2@\text{CoO}$ with sulfur loadings of ~60 wt.% exhibit a high specific capacity of $1500\text{ mAh}\cdot\text{g}^{-1}$ and remains $540\text{ mAh}\cdot\text{g}^{-1}$ after 70 cycles at $100\text{ mA}\cdot\text{g}^{-1}$ in 1 M $\text{Mg}(\text{TFSI})_2\text{-AlCl}_3/\text{DME}$ electrolyte.

To date, much work has been done to enhance electrochemical performance by using Cu current collector, with significant benefits achieved [34,63,66–71]. In a study by Nu et al. [72], Mg-S cell cycling performance with copper and stainless steel current col-

lectors was compared. The stainless steel collector provided a discharge capacity of only $9 \text{ mAh} \cdot \text{g}^{-1}$ but $200 \text{ mAh} \cdot \text{g}^{-1}$ was found with copper in APC electrolyte. Lee et al. [63] described the reaction mechanisms of S_8 with Cu in rechargeable Mg-S batteries with boron-centered anion-based magnesium electrolytes (BCM) electrolyte. Mg-S batteries on the basis of that cathode electrodes with an Al current collector gave capacities of only $50 \text{ mAh} \cdot \text{g}^{-1}$ at 0.02 C, while a Cu current collector provided a reversible capacity of $720 \text{ mAh} \cdot \text{g}^{-1}$, accompanied by an obvious discharge plateau of 1V (Figure 9e). Lee et al. deduced that in the initial stage of discharge, S_8 was reduced to MgS_8 , and then continued to react with Cu metal to form SCSs and Cu^+ , and then SCSs reacted with Cu^+ and Cu to form Cu_2S ; finally, Cu_2S was reduced to Cu and MgS (Figure 10a). During the charging process, Cu nanowires formed after discharge, and the unreacted Cu_2S was evenly distributed around the MgS, helping to enhance positive electrode electronic conductivity. Simultaneously, some Cu^+ diffuses, forming Cu_2S particles in MgS, promoting the charging reaction (Figure 10b). Although copper collectors can significantly improve electrochemical performance, collector corrosion during discharge can be fatal to the working life and safety. The SEM images in Figure 10c–f show the morphology of Cu collectors in different states. After the first cycle, the microscopic surface coarsens and significant corrosion occurs, which is fatal to electrode structures. He et al. [67] employed Cu nanoparticles grown on carbon nanofiber (CNF) as a sulfur host to explore the influence of different Cu loadings on Mg-S cells and found that with Cu:S mass ratios from 1:4 to 1:1, the cycling and rate performances of Mg-S cells gradually became better. However, excessive Cu additive can be expected to cause a loss of energy density, and the cost of adding copper to the cathode may limit the practicality of such Mg-S cells. In principle, the introduction of various forms of copper, e.g., Cu single atoms, Cu nanoparticles, Cu nanowires, and other structures improves the utilization of Cu [73]. It is also possible to synthesize copper derivatives such as CuS_x , CuSe_x , CuP_x , etc., to obtain higher reaction kinetic performances [45,74,75].

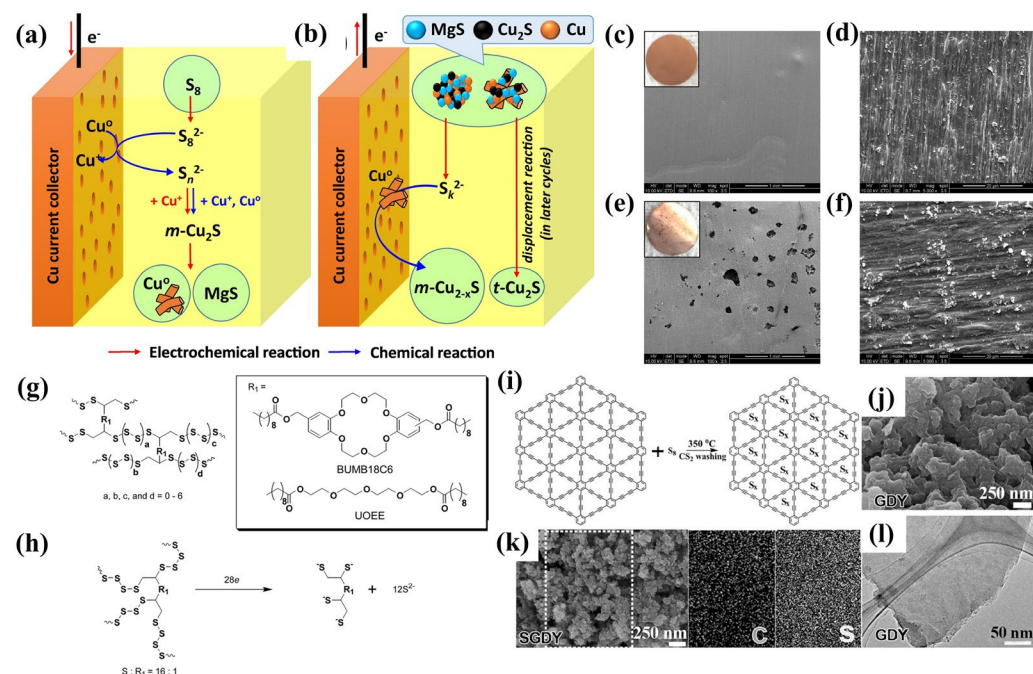


Figure 10. The proposed reaction mechanism diagram during (a) discharge and (b) charge. SEM of the Cu collector in Mg–S batteries: (c,d) original electrode, and (e,f) fully charged electrode after the first cycle [63]. (g) Structures of BUMB18C6 and UOEE. (h) Electrochemical reaction principles of sulfur–containing composites [76]. (i) The preparation process of SGDY, and corresponding (j) SEM image, (k) SEM images and corresponding element mapping, (l) HRTEM image [77].

3.3. Covalently Bonded Sulfur Cathode

Polymers containing S-S bonds may become a promising direction since the design principle for Mg-S batteries is similar to that of Li-S batteries [78,79]. In 2007, Feng [80] and NuLi [81] first used organosulfur compounds with S-S bonds in Mg-S batteries. Nevertheless, all of these organosulfur compounds exhibit poor electrochemical performance, which could be attributed to the mismatched electrolyte. As a follow-up, S-bis(undec-10-enoyloxymethylbenzo)-18-crown-6-ether (BUMB18C6) and S-oxybis (2,1-ethanediylloxy-2,1-ethane-diyl) ester (UOEE) (Figure 10g) were prepared by a simple solvothermal method [76]. Figure 10h shows the suggested mechanism of formation for these types of compounds during discharge. S-BUMB18C6 has similar initial discharge capacities to S-UOEE, while the cycling performance of S-BUMB18C6 is better than the S-UOEE electrode, which can be ascribed to the ionic conduction path created by the crown ether unit in S-BUMB18C6.

Graphdiyne (GDY) has a unique structure with uniformly distributed pores of 5.42 Å diameter and 0.365 nm interplanar spacing formed by benzene rings and connected by butadiene bonds. Du et al. [77] successfully synthesized sulfide graphdiyne (SGDY) by thermally inducing a reaction with S_8 forming SCSs (S_x , $1 < x < 5$) at 350 °C, which anchored in the GDY triangular pores (Figure 10i–l). Both C-S bonds and S-S bonds are observed in SGDY, but not S_8 . However, acceptable electrochemical performance was only achieved by using LiCl additives in the electrolyte, with a specific capacity of 1125 mAh·g⁻¹ and 41% capacity retention after 36 cycles at 50 mA·g⁻¹, which may be related to the slow dynamic performance of Mg²⁺ with SCSs in the solid state.

Sulfurized polyacrylonitrile (SPAN) is one of the most promising covalently bonded sulfur cathode materials for Li-S batteries, with the ability to chemically bind sulfur to the polymer backbone. SPAN was first used in magnesium-sulfur batteries in 2007 and was prepared by thermal treatment of PAN/ S_8 mixtures [80]. In one study on SPAN utility for Mg-S cells, Wang and co-workers [82] combined SPAN with 0.8 M Mg[B(hfip)₄]₂ in DME/TEG. They observed a discharge capacity of 550 mAh·g⁻¹ (ca. 207 mAh·g⁻¹_{SPAN}) and stable cycling over 70 cycles at 0.033 C (Figure 11a,b). Mg-SPAN cells with Mg²⁺/Li⁺ hybrid electrolytes were also explored [42,43]. Cycling for 100 cycles at 1.67 mA/cm² with a capacity of 1100 mAh·g⁻¹ and a Coulombic efficiency >99.9% (Figure 11c,d) [42]. EIS demonstrated that the lithium salts effectively reduce resistance and overpotential when the electrolyte contains polysulfides and sulfides.

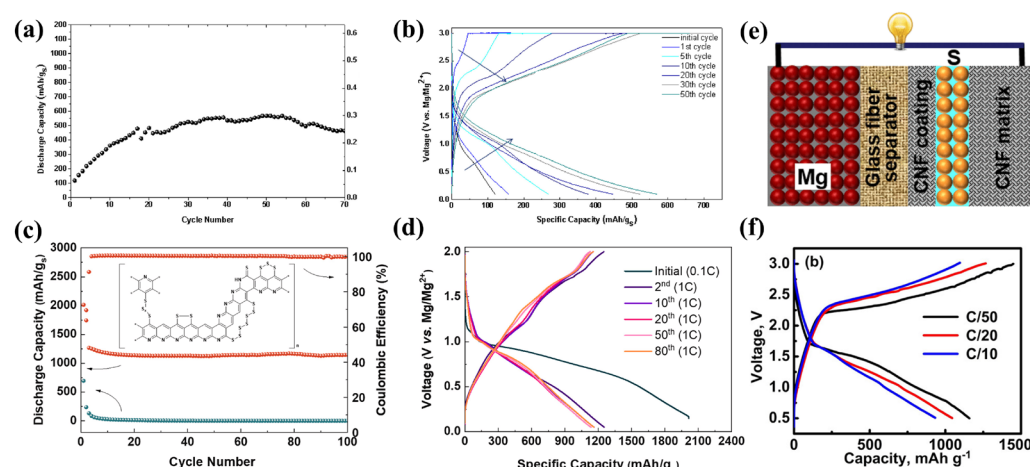


Figure 11. (a) Cycling performance of SPAN cathode in 0.8 M Mg[B(hfip)₄]₂ electrolyte at 0.033 C and corresponding (b) discharge–charge profile [82]. (c) Cycling performance of SPAN cathode with the Mg²⁺/Li⁺ electrolyte (orange) and the Mg²⁺ electrolyte (green) at 1 C (inset: chemical structure of SPAN). (d) Discharge–charge profile of SPAN in 0.2 M Mg(CF₃SO₃)₂–0.4 M MgCl₂–0.4 M AlCl₃–1.6 M LiCF₃SO₃ electrolyte [42]. (e) Schematic of a CNF-coated separator in Mg–S cell and the corresponding (f) discharge–charge profile in Mg(HMDS)₂–MgCl₂–AlCl₃ electrolyte [56].

Selenium-sulfur composites have been used to enhance cathode electrical conductivity and mitigate the polysulfide shuttle problem [46,83–85]. For example, Du and colleagues [46] explored selenium-sulfur (SeS_2) in Mg-S batteries targeting high energy and efficient kinetics. $\text{SeS}_2/\text{CMK-3}$ cathode with a mass loading of $\sim 2 \text{ mg}\cdot\text{cm}^{-2}$ shows $\sim 1000 \text{ mAh}\cdot\text{g}^{-1}$ discharge capacity at $112 \text{ mA}\cdot\text{g}^{-1}$, and lower charge-discharge polarization voltage than $\text{Se}/\text{CMK-3}$ and $\text{S}/\text{CMK-3}$. Hence, selenium can act as a eutectic promoter, greatly increasing the electronic conductivity of sulfur compounds and leading to lower voltage polarization and higher sulfur utilization.

3.4. Interlayer Modification on Cathode Side

The introduction of functionalized separators on the cathode side also offers significant suppression of the polysulfide shuttle effect [19,44,49,86]. Yu [56] found that an active CNF-coated separator can act both as an absorption host to trap soluble polysulfides and as a current collector to enhance the conversion of polysulfides, which delivers a remarkable discharge capacity of $1200 \text{ mAh}\cdot\text{g}^{-1}$ in Mg-S cells (Figure 11e,f).

Because Mo_6S_8 offers a combination of high electronic, high ionic conductivity, and high affinity for polysulfides, Wang et al. coated Mo_6S_8 ($0.2\text{--}0.3 \text{ mg}\cdot\text{cm}^{-2}$) on a Celgard separator (CG@CP) to effectively enhance the conversion of polysulfides [44]. In Mg-S pouch cell tests, the initial discharge capacity reached $510 \text{ mAh}\cdot\text{g}^{-1}$, and the reversible capacity was 182 and $103 \text{ mAh}\cdot\text{g}^{-1}$ after 50 and 100 cycles, respectively (Figure 12a–c). CG@CP promotes the reversibility of the S_8 redox chemistry and maintains cycling stability, as confirmed by XPS analysis and ex situ Raman measurements (Figure 12d,e). Analogously, Xu et al. [19] promoted the performance of Mg-S cells by activating unreacted MgS and Mg_3S_8 species using a TiS_2 coated separator ($\text{TiS}_2@\text{separator}$) with a TiS_2 mass loading of $0.15 \text{ mg}\cdot\text{cm}^{-2}$ (Figure 12f). The cells with $\text{TiS}_2@\text{separators}$ had a reversible capacity of $900 \text{ mAh}\cdot\text{g}^{-1}$ after 30 cycles at $83 \text{ mA}\cdot\text{g}^{-1}$ with a sulfur loading of $1 \text{ mg}\cdot\text{cm}^{-2}$ (Figure 12g). According to DFT calculations, the decomposition energy barrier for chemisorbed MgS on TiS_2 is reduced by 0.88 eV compared to graphene, thus Ti_2S could facilitate the conversion of SCSs to LCSs (Figure 12h). Recently, Nu's group [45] found that metal phosphides (Cu_3P) also exhibit high conductivity and electrocatalytic activity, which is favorable for Mg-S cells. In long-term tests, pouch cells with $\text{Cu}_3\text{P}@$ carbon separators exhibited a reversible capacity of over $200 \text{ mAh}\cdot\text{g}^{-1}$ after 100 cycles. Zhou et al. [86] designed an advanced metal-sulfur cell Janus separator using intrinsically safe polyimide films, highly reactive metallic copper nanowires, and a rigid solid electrolyte. The assembled Mg-S battery delivered a high capacity of $915 \text{ mAh}\cdot\text{g}^{-1}$ at 50°C even after 25 cycles.

In addition to modifications on cathode side separators, interface modification between the cathode and electrolyte can also improve polysulfide shuttling issues. Cui's group [46] first applied copper foam as an interlayer between $\text{SSe}_2/\text{CMK-3}$ cathodes and separators, boosting the overall charge-discharge kinetics by promoting reversible reactions between copper sulfide/copper selenide and magnesium species. It was demonstrated by ex situ XRD and XPS that the rapid chemical reactions between the polysulfide capture layer of copper foam and S_x^{2-} accelerate the discharge process and improve the utilization of cathode material. Karger's group [87] investigated graphene-PAN-coated carbon cloth as a multifunctional interlayer to suppress self-discharge and adsorbing polysulfides, showing lower polarization and nearly $380 \text{ mAh}\cdot\text{g}^{-1}$ after 150 cycles. Design approaches like these provide a promising way to effectively improve the performance of metal-sulfur batteries.

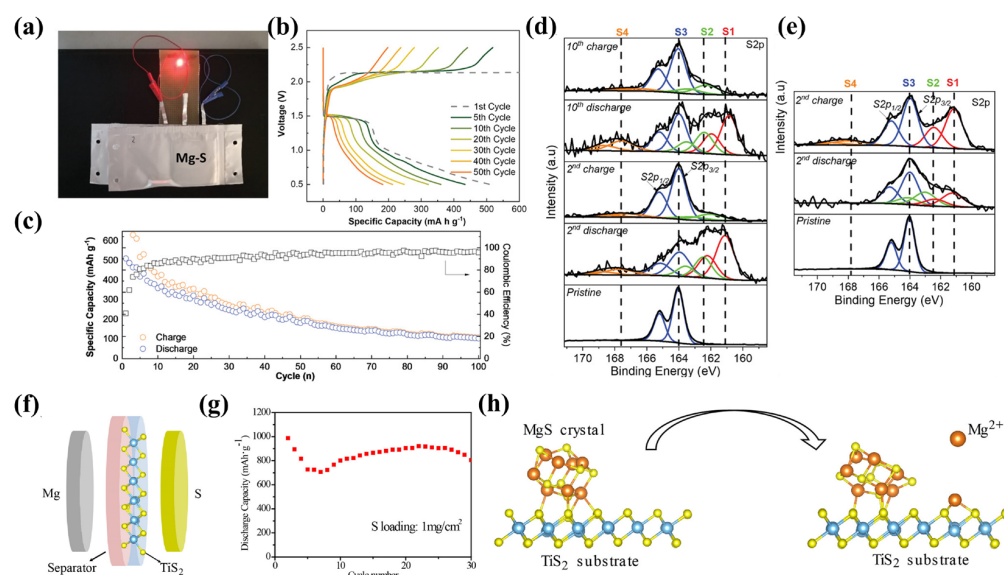


Figure 12. (a) Light up LED test by connecting two Mg–S pouch cells with CG@CP. Electrochemical performance of Mg–S pouch cell with CG@CP: (b) discharge–charge profiles, (c) Long term cycling at 0.05 C. (d) S 2p XPS of the S/KB cathodes (d) with CG@CP and (e) without CG@CP at various cycling state [44]. Mg–S battery with TiS₂@separator: (f) Structure diagram. (g) Cycling stability. (h) TiS₂ catalysis in Mg–S cells [19].

4. Research Progresses on Non-Nucleophilic Electrolytes

The compatibility of the electrolyte with the sulfur cathode in Mg–S batteries is critical to battery performance given the electrophilic nature of sulfur cathodes. In addition, Mg can react with ester, sulphone, amides, and nitriles to produce passivated films. Therefore, ether-based solvents are often used in RMBs systems. Anions with solvation structure play a crucial role in the electrochemical performance of electrolytes [88]. BF₄[−], PF₆[−], AsF₆[−], and ClO₄[−] will decompose on Mg metal and form stable MgO, Mg(OH)₂, MgF₂, etc., which impede Mg²⁺ diffusion, resulting in irreversible dissolution and deposition. As a result, electrolytes such as sulfonate and boron-based compounds are promising options due to their stability in relation to magnesium metal [89].

Non-nucleophilic electrolytes such as MgCl₂(HMDS)-AlCl₃ were first proposed by Kim and Muldoon et al. in 2011 [11]. They mixed non-nucleophilic HMDS·MgCl with AlCl₃ in a ratio of 3:1 in THF to form the [Mg₂(μ-Cl)₃·6THF]⁺ cation and the [HMDS_n·AlCl_{4-n}][−] anion as the electrochemically active roles of the electrolyte, which has a voltage stability of 3.2 V vs. Mg and is compatible with the electrophilic sulfur cathode. As shown in Figure 13a, the central magnesium atoms are coordinated to two octahedra by three Cl atoms, while the THF molecules are linked to the other triple positions on each magnesium atom by oxygen atoms. However, MgCl₂(HMDS)-AlCl₃ electrolyte cannot prevent sulfide dissolution, resulting in a fast capacity decay of 390 mA h·g^{−1} after the first cycle of 1200 mA h·g^{−1} (Figure 13b). To avoid the formation of the HMDSAlCl₃ by-product, they introduced MgCl₂ to convert it into [HMDSAlCl₃][−] [16]. In 2014, Ha et al. [54] reported that Mg(TFSI)₂ in a glyme/diglyme solvent allows the electrochemical conversion of sulfur to MgS in Mg/CMK3-S batteries, but faces a rapid capacity decay after the initial cycle (Figure 13b) and 2.0 V large overpotential before activation. To alleviate the passivation of the Mg anode caused by H₂O and impurities, MgCl[−] was introduced [35,90,91]. Gao et al. [35] used 1M Mg(TFSI)₂-MgCl₂ and obtained cycling stabilities exceeding 100 cycles (Figure 13c). However, Both MgCl₂(HMDS)-AlCl₃, Mg(TFSI)₂-MgCl₂ and Mg(TFSI)₂-MgCl₂-AlCl₃ electrolytes are corrosive to metal current collectors, severely limiting their large-scale application [92]. Accordingly, there is an urgent need for the development of non-corrosive and high voltage electrolytes for Mg–S batteries.

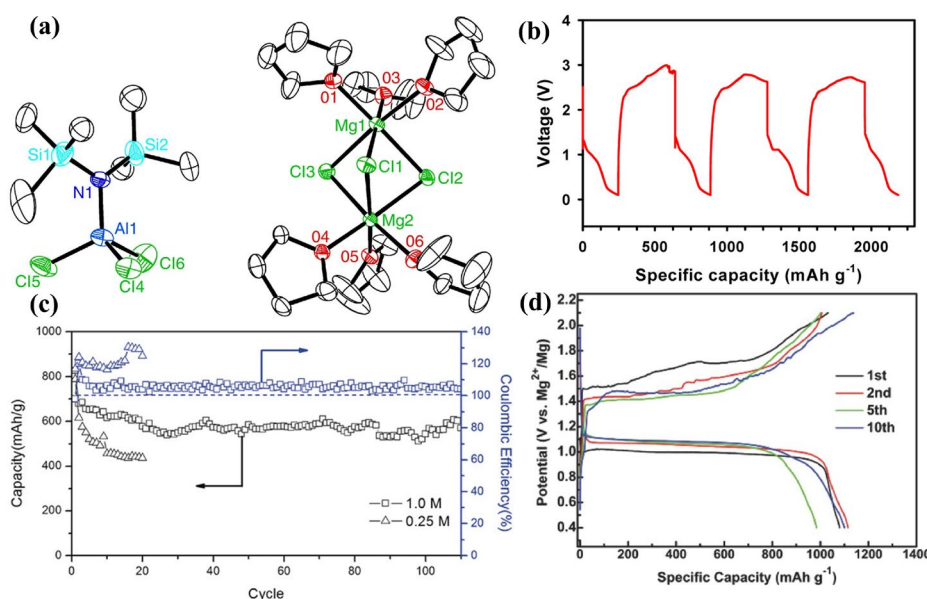


Figure 13. (a) Crystal structure of $[Mg_2(\mu-Cl)_3 \cdot 6THF][HMDSAlCl_3]$ and corresponding (b) charge–discharge curves [11]. (c) Long–term cycling of Mg–S cells with $MgTFSI_2$ – $MgCl_2$ /DME electrolyte [35]. (d) Charge–discharge curves of Mg–S cells with BCM electrolyte at $0.05 \text{ A} \cdot \text{g}^{-1}$ [93].

$Mg(BH_4)_2$ as a hydrogen storage material was first applied in RMBs as a borohydride electrolyte in 2012 [94]. However, the oxidation potential of 1.7 V limits its application in Mg–S cells. Later, Zhao-Karger et al. developed an electrolyte tetrakis(hexafluoroisopropoxy) borate ($Mg[B(hfip)_4]_2$) with boron as the central atom [17,55]. $Mg[B(hfip)_4]_2$ has promising electrochemical properties, high oxidative stability (4.3 V with stainless steel), high electrical conductivity ($6.8 \text{ mS} \cdot \text{cm}^{-1}$ at 25°C), and excellent Mg stripping/plating coulombic efficiency (>98%), and most importantly, good chemical compatibility making it well suited for high energy Mg cells. Cui et al. used THFPB with magnesium salts such as MgF_2 and MgO as electrolytes for Mg–S batteries [93,95]. The oxidative voltage of BCM electrolyte reached 3.5 V (vs. Mg/Mg^{2+}), the ionic conductivity is $1.1 \text{ mS} \cdot \text{cm}^{-1}$, and the first discharge specific capacity reached $1081 \text{ mAh} \cdot \text{g}^{-1}$ (Figure 13d).

In addition, electrolyte additives are also introduced by researchers as a means to improve the performance of electrolytes. It was found that the use of LiCl [96,97] and YCl_3 [98] as additives can effectively improve the cycle life and rate performance of Mg–S batteries. These additives effectively lower the overpotential and inhibit polysulfide shuttling. Thus, magnesium-sulfur batteries with high energy densities can be produced in the near future by adopting non-nucleophilic electrolytes with proper additives.

5. Conclusions

Since the potential of Mg–S batteries was first identified, researchers have carried out extensive efforts to clarify and detail their electrochemical behavior seeking ways to realize the anticipated performance. Although similar to Li–S batteries, numerous difficulties remain unresolved. First, the solubility of magnesium polysulfides is lower than lithium polysulfides in typical electrolytes, but a serious shuttle problem exists, likely related to the slow kinetics of Mg^{2+} diffusion or the special characteristics of some intermediates. Second, the exact mechanism of the rapid capacity decay remains unknown. There are reports attributing this to the formation of electrochemically inert MgS and MgS_x by the first discharge, and there are also reports indicating that the dissolution and shuttling of sulfur and polysulfides is the main reason [17,19]. Third, the severe self-discharge behavior of Mg–S batteries (up to 90% capacity loss) needs to be more deeply investigated. To date, this serious self-discharge has attracted great interest and must be addressed to commercialize Mg–S batteries. The application of operando UV–Vis [23],

XAS [19,21], and Raman spectroscopies [24] to reveal the potential mechanisms whereby Mg-S batteries function remains a rich area in need of more attention. The operando Raman mapping technique allows real-time monitoring of the in-plane distribution of ions and the evolution of the chemical environment [99]. In addition, RIXS and XANES assays can provide an accurate characterization of elemental valence and coordination environments, compensating for the shortcomings of XRD and XPS [21]. Finally, there is a lack of quantitative models proposed for Mg-S batteries.

In terms of the cathode side, multiple efforts have been devoted to exploring porous and high-conductivity materials to anchor sulfur and polysulfides and improve the kinetic performance of active materials. Nevertheless, reported sulfur loadings are generally at $1 \text{ mg}\cdot\text{cm}^2$, which is far below the requirements of commercial applications. In addition, the large overpotential causes ultra-low energy efficiencies, as low as 30%. Hence, achieving high performance and high surface loading is one important direction for cathode material development. For interlayers between the cathode and separator, TiS_2 [19], Mo_6S_8 [44], Cu_3P [45], and graphene [49] can effectively mitigate polysulfide shuttling by physical limitations or catalysis. However, the added volume and mass will reduce energy densities. Therefore, the key challenge is to develop coatings or interlayers that can effectively prevent sulfur and polysulfide from shuttling, have low mass and volume, and are able to selectively conduct magnesium ions. Moreover, it is important to explore the underlying mechanisms behind the improved electrical performance.

With regards to electrolytes, developing non-nucleophilic non-corrosive electrolytes is the future direction. Boron-based electrolytes with large anions can effectively reduce the Mg^{2+} dissociation energy but also increases electrolyte mass. Additionally, suitable additives can alleviate negative electrode passivation, form a protective layer, etc. In principle, all-solid-state Mg-S cells are one effective solution to address polysulfide migration [100,101]. However, this approach likely suffers from slower redox kinetics and the sluggish migration of magnesium ions. On this account, quasi-solid-state electrolytes may offer a compromise.

In summary, Mg-S batteries still need further optimization to meet requirements for practical applications. We hope this review will provide some insight into the development of Mg-S batteries.

Author Contributions: Conceptualization, J.X.Z. and Y.Y.Y.; methodology, J.X.Z.; validation, J.X.Z., X.Y.S. and Y.Z.; formal analysis, Z.L. and H.X.; investigation, Y.Y.Y., X.Y.S. and Y.Z.; resources, J.X.Z.; data curation, Y.Y.Y. and X.Y.S.; writing—original draft preparation, Y.Y.Y., X.Y.S. and Y.Z.; writing—review and editing, J.X.Z., R.M.L., Y.Y.Y., X.Y.S. and Y.Z.; visualization, Y.Y.Y. and X.Y.S.; supervision, J.X.Z.; project administration, J.X.Z.; funding acquisition, J.X.Z. All authors have read and agreed to the published version of the manuscript.

Funding: This research was funded by the National Natural Science Foundation of China (No.52171186), and National Key Research & Development Program of China (No.2022YFB3803700).

Institutional Review Board Statement: Not applicable.

Informed Consent Statement: Not applicable.

Data Availability Statement: Data supporting reporting results are available by request: zoujx@sjtu.edu.cn.

Conflicts of Interest: The authors declare no conflict of interest. Funders have no role in the design of the study; in the collection, analyses, or interpretation of data; in the writing of the manuscript; or in the decision to publish the result.

References

1. Franke, K.; Sensfuß, F.; Bernath, C.; Lux, B. Carbon-neutral energy systems and the importance of flexibility options: A case study in China. *Comput. Ind. Eng.* **2021**, *162*, 107712. [[CrossRef](#)]
2. Liu, J.; Bao, Z.; Cui, Y.; Dufek, E.J.; Goodenough, J.B.; Khalifah, P.; Li, Q.; Liaw, B.Y.; Liu, P.; Manthiram, A.; et al. Pathways for practical high-energy long-cycling lithium metal batteries. *Nat. Energy* **2019**, *4*, 180–186. [[CrossRef](#)]

3. Guo, Y.; Wu, S.; He, Y.-B.; Kang, F.; Chen, L.; Li, H.; Yang, Q.-H. Solid-state lithium batteries: Safety and prospects. *eScience* **2022**, *2*, 138–163. [[CrossRef](#)]
4. Mohtadi, R.; Tutasaus, O.; Arthur, T.S.; Zhao-Karger, Z.; Fichtner, M. The metamorphosis of rechargeable magnesium batteries. *Joule* **2021**, *5*, 581–617. [[CrossRef](#)]
5. Liang, Y.; Dong, H.; Aurbach, D.; Yao, Y. Current status and future directions of multivalent metal-ion batteries. *Nat. Energy* **2020**, *5*, 646–656. [[CrossRef](#)]
6. Tian, H.; Gao, T.; Li, X.; Wang, X.; Luo, C.; Fan, X.; Yang, C.; Suo, L.; Ma, Z.; Han, W.; et al. High power rechargeable magnesium/iodine battery chemistry. *Nat. Commun.* **2017**, *8*, 14083. [[CrossRef](#)] [[PubMed](#)]
7. Blake, I.C. Fiftieth Anniversary: The Anniversary Issue on Primary Cell. *J. Electrochem. Soc.* **1952**, *99*, 202C. [[CrossRef](#)]
8. Gregory, T.D.; Hoffman, R.J.; Winterton, R.C. Nonaqueous Electrochemistry of Magnesium: Applications to Energy Storage. *J. Electrochem. Soc.* **1990**, *137*, 775–780. [[CrossRef](#)]
9. Aurbach, D.; Lu, Z.; Schechter, A.; Gofer, Y.; Gizbar, H.; Turgeman, R.; Cohen, Y.; Moshkovich, M.; Levi, E. Prototype systems for rechargeable magnesium batteries. *Nature* **2000**, *407*, 724–727. [[CrossRef](#)]
10. Mizrahi, O.; Amir, N.; Pollak, E.; Chusid, O.; Marks, V.; Gottlieb, H.; Larush, L.; Zinigrad, E.; Aurbach, D. Electrolyte Solutions with a Wide Electrochemical Window for Rechargeable Magnesium Batteries. *J. Electrochem. Soc.* **2008**, *155*, A103. [[CrossRef](#)]
11. Kim, H.S.; Arthur, T.S.; Allred, G.D.; Zajicek, J.; Newman, J.G.; Rodnyansky, A.E.; Oliver, A.G.; Boggess, W.C.; Muldoon, J. Structure and compatibility of a magnesium electrolyte with a sulphur cathode. *Nat. Commun.* **2011**, *2*, 427. [[CrossRef](#)] [[PubMed](#)]
12. Guo, Z.; Zhao, S.; Li, T.; Su, D.; Guo, S.; Wang, G. Recent Advances in Rechargeable Magnesium-Based Batteries for High-Efficiency Energy Storage. *Adv. Energy Mater.* **2020**, *10*, 1903591. [[CrossRef](#)]
13. Bitenc, J.; Dominko, R. Opportunities and Challenges in the Development of Cathode Materials for Rechargeable Mg Batteries. *Front. Chem.* **2018**, *6*, 634. [[CrossRef](#)] [[PubMed](#)]
14. Xu, H.; Li, Y.; Zhu, D.; Li, Z.; Sun, F.; Zhu, W.; Chen, Y.; Zhang, J.; Ren, L.; Zhang, S.; et al. Synchrotron Radiation Spectroscopic Studies of Mg²⁺ Storage Mechanisms in High-Performance Rechargeable Magnesium Batteries with Co-Doped FeS₂ Cathodes. *Adv. Energy Mater.* **2022**, *12*, 2201608. [[CrossRef](#)]
15. Li, Z.; Yao, Y.; Li, B.; Wang, L.; Xu, H.; Chong, L.; Zou, J. Rechargeable magnesium batteries: Development, opportunities and challenges. *Chin. J. Nonferrous Met.* **2021**, *31*, 3192–3216.
16. Zhao-Karger, Z.; Zhao, X.; Wang, D.; Diemant, T.; Behm, R.J.; Fichtner, M. Performance Improvement of Magnesium Sulfur Batteries with Modified Non-Nucleophilic Electrolytes. *Adv. Energy Mater.* **2015**, *5*, 1401155. [[CrossRef](#)]
17. Zhao-Karger, Z.; Liu, R.; Dai, W.; Li, Z.; Diemant, T.; Vinayan, B.P.; Bonatto Minella, C.; Yu, X.; Manthiram, A.; Behm, R.J.; et al. Toward Highly Reversible Magnesium-Sulfur Batteries with Efficient and Practical Mg[B(hfip)₄]₂ Electrolyte. *ACS Energy Lett.* **2018**, *3*, 2005–2013. [[CrossRef](#)]
18. Gao, T.; Ji, X.; Hou, S.; Fan, X.; Li, X.; Yang, C.; Han, F.; Wang, F.; Jiang, J.; Xu, K.; et al. Thermodynamics and Kinetics of Sulfur Cathode during Discharge in MgTFSI₂-DME Electrolyte. *Adv. Mater.* **2018**, *30*, 1704313. [[CrossRef](#)]
19. Xu, Y.; Ye, Y.; Zhao, S.; Feng, J.; Li, J.; Chen, H.; Yang, A.; Shi, F.; Jia, L.; Wu, Y.; et al. In Situ X-ray Absorption Spectroscopic Investigation of the Capacity Degradation Mechanism in Mg/S Batteries. *Nano Lett.* **2019**, *19*, 2928–2934. [[CrossRef](#)]
20. Du, W.; Hao, Z.; Iacoviello, F.; Sheng, L.; Guan, S.; Zhang, Z.; Brett, D.J.L.; Wang, F.R.; Shearing, P.R. A Multiscale X-Ray Tomography Study of the Cycled-Induced Degradation in Magnesium-Sulfur Batteries. *Small Methods* **2021**, *5*, 2001193. [[CrossRef](#)]
21. Robba, A.; Vizintin, A.; Bitenc, J.; Mali, G.; Arčon, I.; Kavčič, M.; Žitnik, M.; Bučar, K.; Aquilanti, G.; Martineau-Corcos, C.; et al. Mechanistic Study of Magnesium-Sulfur Batteries. *Chem. Mater.* **2017**, *29*, 9555–9564. [[CrossRef](#)]
22. Yu, X.; Manthiram, A. Ambient-Temperature Energy Storage with Polyvalent Metal-Sulfur Chemistry. *Small Methods* **2017**, *1*, 1700217. [[CrossRef](#)]
23. Haecker, J.; Duc Hien, N.; Rommel, T.; Zhao-Karger, Z.; Wagner, N.; Friedrich, K.A. Operando UV/vis Spectroscopy Providing Insights into the Sulfur and Polysulfide Dissolution in Magnesium-Sulfur Batteries. *ACS Energy Lett.* **2022**, *7*, 1–9. [[CrossRef](#)]
24. Bhardwaj, R.K.; Gomes, R.; Bhattacharyya, A.J. Probing the Polysulfide Confinement in Two Different Sulfur Hosts for a Mg|S Battery Employing Operando Raman and Ex-Situ UV-Visible Spectroscopy. *J. Phys. Chem. Lett.* **2022**, *13*, 1159–1164. [[CrossRef](#)]
25. Laskowski, F.A.L.; Stradley, S.H.; Qian, M.D.; See, K.A. Mg Anode Passivation Caused by the Reaction of Dissolved Sulfur in Mg-S Batteries. *ACS Appl. Mater. Inter.* **2021**, *13*, 29461–29470. [[CrossRef](#)]
26. Zhang, R.; Cui, C.; Xiao, R.; Li, R.; Mu, T.; Huo, H.; Ma, Y.; Yin, G.; Zuo, P. Interface regulation of Mg anode and redox couple conversion in cathode by copper for high-performance Mg-S battery. *Chem. Eng. J.* **2023**, *451*, 138663. [[CrossRef](#)]
27. Vinayan, B.P.; Zhao-Karger, Z.; Diemant, T.; Chakravadhanula, V.S.K.; Schwarzburger, N.I.; Cambaz, M.A.; Behm, R.J.; Kuebel, C.; Fichtner, M. Performance study of magnesium-sulfur battery using a graphene based sulfur composite cathode electrode and a non-nucleophilic Mg electrolyte. *Nanoscale* **2016**, *8*, 3296–3306. [[CrossRef](#)]
28. Dan-Thien, N.; Horia, R.; Eng, A.Y.S.; Song, S.-W.; Seh, Z.W. Material design strategies to improve the performance of rechargeable magnesium-sulfur batteries. *Mater. Horiz.* **2021**, *8*, 830–853. [[CrossRef](#)]
29. Schmidt, A.; Koger, H.; Barthelemy, A.; Studer, G.; Esser, B.; Krossing, I. Is One of the Least Coordinating Anions Suitable to Serve as Electrolyte Salt for Magnesium-Ion Batteries? *Batter. Supercaps* **2022**, *5*, e202200340. [[CrossRef](#)]
30. Fan, H.; Zhao, Y.; Xiao, J.; Zhang, J.; Wang, M.; Zhang, Y. A non-nucleophilic gel polymer magnesium electrolyte compatible with sulfur cathode. *Nano Res.* **2020**, *13*, 2749–2754. [[CrossRef](#)]

31. Wang, L.; Li, Z.; Meng, Z.; Xiu, Y.; Dasari, B.; Zhao-Karger, Z.; Fichtner, M. Designing gel polymer electrolyte with synergistic properties for rechargeable magnesium batteries. *Energy Storage Mater.* **2022**, *48*, 155–163. [[CrossRef](#)]
32. Xiao, J.; Zhang, X.; Fan, H.; Zhao, Y.; Su, Y.; Liu, H.; Li, X.; Su, Y.; Yuan, H.; Pan, T.; et al. Stable Solid Electrolyte In Situ Formed on Magnesium-Metal Anode by using a Perfluorinated Alkoxide-Based All-Magnesium Salt Electrolyte. *Adv. Mater.* **2022**, *34*, 2203783. [[CrossRef](#)] [[PubMed](#)]
33. Muthuraj, D.; Ghosh, A.; Kumar, A.; Mitra, S. Nitrogen and Sulfur Doped Carbon Cloth as Current Collector and Polysulfide Immobilizer for Magnesium-Sulfur Batteries. *Chemelectrochem* **2019**, *6*, 684–689. [[CrossRef](#)]
34. Wang, W.; Yuan, H.; NuLi, Y.; Zhou, J.; Yang, J.; Wang, J. Sulfur@microporous Carbon Cathode with a High Sulfur Content for Magnesium-Sulfur Batteries with Nucleophilic Electrolytes. *J. Phys. Chem. C* **2018**, *122*, 26764–26776. [[CrossRef](#)]
35. Gao, T.; Hou, S.; Wang, F.; Ma, Z.; Li, X.; Xu, K.; Wang, C. Reversible S_0/MgS_x Redox Chemistry in a $MgTFSI_2/MgCl_2/DME$ Electrolyte for Rechargeable Mg/S Batteries. *Angew. Chem.* **2017**, *129*, 13711–13715. [[CrossRef](#)]
36. Muthuraj, D.; Pandey, M.; Krishna, M.; Ghosh, A.; Sen, R.; Johari, P.; Mitra, S. Magnesium polysulfide catholyte (MgS_x): Synthesis, electrochemical and computational study for magnesium-sulfur battery application. *J. Power Sources* **2021**, *486*, 229326. [[CrossRef](#)]
37. Lee, M.; Jeong, M.; Nam, Y.S.; Moon, J.; Lee, M.; Lim, H.D.; Byun, D.; Yim, T.; Oh, S.H. Nitrogen-doped graphitic mesoporous carbon materials as effective sulfur imbibition hosts for magnesium-sulfur batteries. *J. Power Sources* **2022**, *535*, 231471. [[CrossRef](#)]
38. Kaland, H.; Haskjold Fagerli, F.; Hadler-Jacobsen, J.; Zhao-Karger, Z.; Fichtner, M.; Wiik, K.; Wagner, N.P. Performance Study of MXene/Carbon Nanotube Composites for Current Collector- and Binder-Free Mg-S Batteries. *Chemsuschem* **2021**, *14*, 1864–1873. [[CrossRef](#)]
39. Vinayan, B.P.; Euchner, H.; Zhao-Karger, Z.; Cambaz, M.A.; Li, Z.; Diemant, T.; Behm, R.J.; Gross, A.; Fichtner, M. Insights into the electrochemical processes of rechargeable magnesium-sulfur batteries with a new cathode design. *J. Mater. Chem. A* **2019**, *7*, 25490–25502. [[CrossRef](#)]
40. Ford, H.O.; Doyle, E.S.; He, P.; Boggess, W.C.; Oliver, A.G.; Wu, T.; Sterbinsky, G.E.; Schaefer, J.L. Self-discharge of magnesium-sulfur batteries leads to active material loss and poor shelf life. *Energy Environ. Sci.* **2021**, *14*, 890–899. [[CrossRef](#)]
41. Richter, R.; Hacker, J.; Zhao-Karger, Z.; Danner, T.; Wagner, N.; Fichtner, M.; Friedrich, K.A.; Latz, A. Insights into Self-Discharge of Lithium- and Magnesium-Sulfur Batteries. *ACS Appl. Energy Mater.* **2020**, *3*, 8457–8474. [[CrossRef](#)]
42. Wang, P.; Kuester, K.; Starke, U.; Liang, C.; Niewa, R.; Buchmeiser, M.R. Performance enhancement of rechargeable magnesium-sulfur batteries based on a sulfurized poly(acrylonitrile) composite and a lithium salt. *J. Power Sources* **2021**, *515*, 230604. [[CrossRef](#)]
43. Zhang, S.; Ren, W.; NuLi, Y.; Wang, B.; Yang, J.; Wang, J. Sulfurized-Pyrolyzed Polyacrylonitrile Cathode for Magnesium-Sulfur Batteries Containing Mg^{2+}/Li^+ Hybrid Electrolytes. *Chem. Eng. J.* **2022**, *427*, 130902. [[CrossRef](#)]
44. Wang, L.; Jankowski, P.; Njel, C.; Bauer, W.; Li, Z.; Meng, Z.; Dasari, B.; Vegge, T.; Lastra, J.M.G.; Zhao-Karger, Z.; et al. Dual Role of Mo_6S_8 in Polysulfide Conversion and Shuttle for Mg-S Batteries. *Adv. Sci.* **2022**, *9*, 2104605. [[CrossRef](#)] [[PubMed](#)]
45. Yang, Y.; Fu, W.; Zhang, D.; Ren, W.; Zhang, S.; Yan, Y.; Zhang, Y.; Lee, S.J.; Lee, J.S.; Ma, Z.F.; et al. Toward High-Performance Mg-S Batteries via a Copper Phosphide Modified Separator. *ACS Nano* **2022**, *17*, 1255–1267. [[CrossRef](#)] [[PubMed](#)]
46. Du, A.; Zhao, Y.; Zhang, Z.; Dong, S.; Cui, Z.; Tang, K.; Lu, C.; Han, P.; Zhou, X.; Cui, G. Selenium sulfide cathode with copper foam interlayer for promising magnesium electrochemistry. *Energy Storage Mater.* **2020**, *26*, 23–31. [[CrossRef](#)]
47. Nakayama, Y.; Matsumoto, R.; Kumagae, K.; Mori, D.; Mizuno, Y.; Hosoi, S.; Kamiguchi, K.; Koshitani, N.; Inaba, Y.; Kudo, Y.; et al. Zinc Blende Magnesium Sulfide in Rechargeable Magnesium-Sulfur Batteries. *Chem. Mater.* **2018**, *30*, 6318–6324. [[CrossRef](#)]
48. Zou, Q.; Sun, Y.; Liang, Z.; Wang, W.; Lu, Y.-C. Achieving Efficient Magnesium-Sulfur Battery Chemistry via Polysulfide Mediation. *Adv. Energy Mater.* **2021**, *11*, 2101552. [[CrossRef](#)]
49. Zhou, X.; Tian, J.; Hu, J.; Li, C. High Rate Magnesium-Sulfur Battery with Improved Cyclability Based on Metal-Organic Framework Derivative Carbon Host. *Adv. Mater.* **2018**, *30*, 1704166. [[CrossRef](#)] [[PubMed](#)]
50. Sungjemmenla; Soni, C.B.; Vineeth, S.K.; Kumar, V. Exploration of the Unique Structural Chemistry of Sulfur Cathode for High-Energy Rechargeable Beyond-Li Batteries. *Adv. Energy Sustain. Res.* **2022**, *3*, 2100157. [[CrossRef](#)]
51. Elazari, R.; Salitra, G.; Garsuch, A.; Panchenko, A.; Aurbach, D. Sulfur-impregnated activated carbon fiber cloth as a binder-free cathode for rechargeable Li-S batteries. *Adv. Mater.* **2011**, *23*, 5641–5644. [[CrossRef](#)] [[PubMed](#)]
52. Ji, X.; Lee, K.T.; Nazar, L.F. A highly ordered nanostructured carbon-sulphur cathode for lithium-sulphur batteries. *Nat. Mater.* **2009**, *8*, 500–506. [[CrossRef](#)] [[PubMed](#)]
53. Du, A.; Zhang, Z.; Qu, H.; Cui, Z.; Qiao, L.; Wang, L.; Chai, J.; Lu, T.; Dong, S.; Dong, T.; et al. An efficient organic magnesium borate-based electrolyte with non-nucleophilic characteristics for magnesium-sulfur battery. *Energy Environ. Sci.* **2017**, *10*, 2616–2625. [[CrossRef](#)]
54. Ha, S.-Y.; Lee, Y.-W.; Woo, S.W.; Koo, B.; Kim, J.-S.; Cho, J.; Lee, K.T.; Choi, N.-S. Magnesium(II) Bis(trifluoromethane sulfonyl) Imide-Based Electrolytes with Wide Electrochemical Windows for Rechargeable Magnesium Batteries. *ACS Appl. Mater. Inter.* **2014**, *6*, 4063–4073. [[CrossRef](#)]
55. Zhao-Karger, Z.; Gil Bardaji, M.E.; Fuhr, O.; Fichtner, M. A new class of non-corrosive, highly efficient electrolytes for rechargeable magnesium batteries. *J. Mater. Chem. A* **2017**, *5*, 10815–10820. [[CrossRef](#)]
56. Yu, X.; Manthiram, A. Performance Enhancement and Mechanistic Studies of Magnesium-Sulfur Cells with an Advanced Cathode Structure. *ACS Energy Lett.* **2016**, *1*, 431–437. [[CrossRef](#)]

57. Zhang, T.; Zhang, L.; Hou, Y. MXenes: Synthesis strategies and lithium-sulfur battery applications. *eScience* **2022**, *2*, 164–182. [[CrossRef](#)]
58. Xu, H.; Zhu, D.; Zhu, W.; Sun, F.; Zou, J.; Laine, R.M.; Ding, W. Rational design of high concentration electrolytes and MXene-based sulfur host materials toward high-performance magnesium sulfur batteries. *Chem. Eng. J.* **2022**, *428*, 131031. [[CrossRef](#)]
59. Zhao, Q.; Wang, R.; Zhang, Y.; Huang, G.; Jiang, B.; Xu, C.; Pan, F. The design of Co_3S_4 @MXene heterostructure as sulfur host to promote the electrochemical kinetics for reversible magnesium-sulfur batteries. *J. Magnes. Alloy.* **2021**, *9*, 78–89. [[CrossRef](#)]
60. Zhang, X.; Wei, Y.; Wang, B.; Wang, M.; Zhang, Y.; Wang, Q.; Wu, H. Construction of Electrocatalytic and Heat-Resistant Self-Supporting Electrodes for High-Performance Lithium-Sulfur Batteries. *Nano-Micro Lett.* **2019**, *11*, 1–17. [[CrossRef](#)]
61. Zhang, S.L.; Guan, B.Y.; Wu, H.B.; Lou, X.W.D. Metal-Organic Framework-Assisted Synthesis of Compact Fe_2O_3 Nanotubes in Co_3O_4 Host with Enhanced Lithium Storage Properties. *Nano-Micro Lett.* **2018**, *10*, 44. [[CrossRef](#)] [[PubMed](#)]
62. Furukawa, H.; Cordova, K.E.; O’Keeffe, M.; Yaghi, O.M. The chemistry and applications of metal-organic frameworks. *Science* **2013**, *341*, 1230444. [[CrossRef](#)] [[PubMed](#)]
63. Lee, B.; Choi, J.; Na, S.; Yoo, D.-J.; Kim, J.H.; Cho, B.W.; Kim, Y.-T.; Yim, T.; Choi, J.W.; Oh, S.H. Critical role of elemental copper for enhancing conversion kinetics of sulphur cathodes in rechargeable magnesium batteries. *Appl. Surf. Sci.* **2019**, *484*, 933–940. [[CrossRef](#)]
64. Sun, J.; Deng, C.; Bi, Y.; Wu, K.-H.; Zhu, S.; Xie, Z.; Li, C.; Amal, R.; Luo, J.; Liu, T.; et al. In Situ Sulfurized Carbon-Confining Cobalt for Long-Life Mg/S Batteries. *ACS Appl. Energy Mater.* **2020**, *3*, 2516–2525. [[CrossRef](#)]
65. Shimokawa, K.; Furuhashi, T.; Kawaguchi, T.; Park, W.-Y.; Wada, T.; Matsumoto, H.; Kato, H.; Ichitsubo, T. Electrochemically synthesized liquid-sulfur/sulfide composite materials for high-rate magnesium battery cathodes. *J. Mater. Chem. A* **2021**, *9*, 16585–16593. [[CrossRef](#)]
66. Robba, A.; Meznar, M.; Vizintin, A.; Bitenc, J.; Bobnar, J.; Arcon, I.; Randon-Vitanova, A.; Dominko, R. Role of Cu current collector on electrochemical mechanism of Mg-S battery. *J. Power Sources* **2020**, *450*, 227672. [[CrossRef](#)]
67. He, P.; Ford, H.O.; Merrill, L.C.; Schaefer, J.L. Investigation of the Effects of Copper Nanoparticles on Magnesium-Sulfur Battery Performance: How Practical Is Metallic Copper Addition? *ACS Appl. Energy Mater.* **2019**, *2*, 6800–6807. [[CrossRef](#)]
68. Zhang, Z.; Chen, B.; Xu, H.; Cui, Z.; Dong, S.; Du, A.; Ma, J.; Wang, Q.; Zhou, X.; Cui, G. Self-Established Rapid Magnesiation/De-Magnesiation Pathways in Binary Selenium-Copper Mixtures with Significantly Enhanced Mg-Ion Storage Reversibility. *Adv. Funct. Mater.* **2018**, *28*, 1701718. [[CrossRef](#)]
69. Zhang, J.; Chang, Z.; Zhang, Z.; Du, A.; Dong, S.; Li, Z.; Li, G.; Cui, G. Current Design Strategies for Rechargeable Magnesium-Based Batteries. *ACS Nano* **2021**, *15*, 15594–15624. [[CrossRef](#)]
70. Cheng, X.; Zhang, Z.; Kong, Q.; Zhang, Q.; Wang, T.; Dong, S.; Gu, L.; Wang, X.; Ma, J.; Han, P.; et al. Highly Reversible Cuprous Mediated Cathode Chemistry for Magnesium Batteries. *Angew. Chem.* **2020**, *132*, 11574–11579. [[CrossRef](#)]
71. Thiele, P.; Neumann, J.; Westphal, A.; Ludwig, R.; Bonsa, A.-M.; Appelhagen, A.; Malcher, P.; Koeckerling, M. Electrical Energy Storage by a Magnesium-Copper-Sulfide Rechargeable Battery. *J. Electrochem. Soc.* **2017**, *164*, A770–A774. [[CrossRef](#)]
72. Zeng, L.; Wang, N.; Yang, J.; Wang, J.; Nuli, Y. Application of a Sulfur Cathode in Nucleophilic Electrolytes for Magnesium/Sulfur Batteries. *J. Electrochem. Soc.* **2017**, *164*, A2504–A2512. [[CrossRef](#)]
73. Xiao, R.; Yu, T.; Yang, S.; Chen, K.; Li, Z.; Liu, Z.; Hu, T.; Hu, G.; Li, J.; Cheng, H.-M.; et al. Electronic structure adjustment of lithium sulfide by a single-atom copper catalyst toward high-rate lithium-sulfur batteries. *Energy Storage Mater.* **2022**, *51*, 890–899. [[CrossRef](#)]
74. He, D.; Xue, P.; Song, D.; Qu, J.; Lai, C. Tri-Functional Copper Sulfide as Sulfur Carrier for High-Performance Lithium-Sulfur Batteries. *J. Electrochem. Soc.* **2017**, *164*, A1499–A1502. [[CrossRef](#)]
75. Yang, D.; Li, M.; Zheng, X.; Han, X.; Zhang, C.; Jacas Biendicho, J.; Llorca, J.; Wang, J.; Hao, H.; Li, J.; et al. Phase Engineering of Defective Copper Selenide toward Robust Lithium-Sulfur Batteries. *ACS Nano* **2022**, *16*, 11102–11114. [[CrossRef](#)] [[PubMed](#)]
76. Itaoka, K.; Kim, I.-T.; Yamabuki, K.; Yoshimoto, N.; Tsutsumi, H. Room temperature rechargeable magnesium batteries with sulfur-containing composite cathodes prepared from elemental sulfur and bis(alkenyl) compound having a cyclic or linear ether unit. *J. Power Sources* **2015**, *297*, 323–328. [[CrossRef](#)]
77. Du, H.; Zhang, Z.; He, J.; Cui, Z.; Chai, J.; Ma, J.; Yang, Z.; Huang, C.; Cui, G. A Delicately Designed Sulfide Graphdiyne Compatible Cathode for High-Performance Lithium/Magnesium-Sulfur Batteries. *Small* **2017**, *13*, 1702277. [[CrossRef](#)]
78. Zheng, N.; Jiang, G.; Chen, X.; Mao, J.; Jiang, N.; Li, Y. Battery Separators Functionalized with Edge-Rich MoS_2/C Hollow Microspheres for the Uniform Deposition of Li_2S in High-Performance Lithium-Sulfur Batteries. *Nano-Micro Lett.* **2019**, *11*, 43. [[CrossRef](#)]
79. Hencz, L.; Chen, H.; Ling, H.Y.; Wang, Y.; Lai, C.; Zhao, H.; Zhang, S. Housing Sulfur in Polymer Composite Frameworks for Li-S Batteries. *Nano-Micro Lett.* **2019**, *11*, 17. [[CrossRef](#)] [[PubMed](#)]
80. Feng, Z.-Z.; Nuli, Y.-N.; Yang, J. Conductive sulfur-containing material/polyaniline composite for cathode material of rechargeable magnesium batteries. *Acta Phys. -Chim. Sin.* **2007**, *23*, 327–331. [[CrossRef](#)]
81. NuLi, Y.; Guo, Z.; Liu, H.; Yang, J. A new class of cathode materials for rechargeable magnesium batteries: Organosulfur compounds based on sulfur-sulfur bonds. *Electrochim. Commun.* **2007**, *9*, 1913–1917. [[CrossRef](#)]
82. Wang, P.; Kappler, J.; Sievert, B.; Haecker, J.; Kuester, K.; Starke, U.; Ziegler, F.; Buchmeiser, M.R. Characteristics of magnesium-sulfur batteries based on a sulfurized poly(acrylonitrile) composite and a fluorinated electrolyte. *Electrochim. Acta* **2020**, *361*, 137024. [[CrossRef](#)]

83. Wu, D.; Ren, W.; Yang, Y.; Wang, J.; NuLi, Y. A Se-Doped S@CMK3 Composite as a High-Performance Cathode for Magnesium-Sulfur Batteries with Mg^{2+}/Li^+ Hybrid Electrolytes. *J. Phys. Chem. C* **2021**, *125*, 25959–25967. [[CrossRef](#)]
84. Zhao, M.; Li, X.-Y.; Chen, X.; Li, B.-Q.; Kaskel, S.; Zhang, Q.; Huang, J.-Q. Promoting the sulfur redox kinetics by mixed organodiselenides in high-energy-density lithium-sulfur batteries. *eScience* **2021**, *1*, 44–52. [[CrossRef](#)]
85. Zhao-Karger, Z.; Lin, X.-M.; Minella, C.B.; Wang, D.; Diemant, T.; Behm, R.J.; Fichtner, M. Selenium and selenium-sulfur cathode materials for high-energy rechargeable magnesium batteries. *J. Power Sources* **2016**, *323*, 213–219. [[CrossRef](#)]
86. Zhou, Z.; Chen, B.; Fang, T.; Li, Y.; Zhou, Z.; Wang, Q.; Zhang, J.; Zhao, Y. A Multifunctional Separator Enables Safe and Durable Lithium/Magnesium-Sulfur Batteries under Elevated Temperature. *Adv. Energy Mater.* **2020**, *10*, 1902023. [[CrossRef](#)]
87. Bosubabu, D.; Li, Z.; Meng, Z.; Wang, L.-P.; Fichtner, M.; Zhao-Karger, Z. Mitigating self-discharge and improving the performance of Mg-S battery in $Mg[B(hfip)_4]_2$ electrolyte with a protective interlayer. *J. Mater. Chem. A* **2021**, *9*, 25150–25159. [[CrossRef](#)]
88. Wang, P.; Buchmeiser, M.R. Rechargeable Magnesium-Sulfur Battery Technology: State of the Art and Key Challenges. *Adv. Funct. Mater.* **2019**, *29*, 1905248. [[CrossRef](#)]
89. Bucur, C.B. *Challenges of a Rechargeable Magnesium Battery: A Guide to the Viability of this Post Lithium-Ion Battery*; Springer International Publishing: Cham, Switzerland, 2018; pp. 11–38.
90. Connell, J.G.; Genorio, B.; Lopes, P.P.; Strmcnik, D.; Stamenkovic, V.R.; Markovic, N.M. Tuning the Reversibility of Mg Anodes via Controlled Surface Passivation by H_2O/Cl^- in Organic Electrolytes. *Chem. Mater.* **2016**, *28*, 8268–8277. [[CrossRef](#)]
91. Cheng, Y.; Stolley, R.M.; Han, K.S.; Shao, Y.; Arey, B.W.; Washton, N.M.; Mueller, K.T.; Helm, M.L.; Sprenkle, V.L.; Liu, J.; et al. Highly active electrolytes for rechargeable Mg batteries based on a $[Mg_2(mu-Cl)2](2+)$ cation complex in dimethoxyethane. *Phys. Chem. Chem. Phys.* **2015**, *17*, 13307–13314. [[CrossRef](#)]
92. Muldoon, J.; Bucur, C.B.; Oliver, A.G.; Zajicek, J.; Allred, G.D.; Boggess, W.C. Corrosion of magnesium electrolytes: Chlorides—The culprit. *Energy Environ. Sci.* **2013**, *6*, 482–487. [[CrossRef](#)]
93. Zhang, Z.; Cui, Z.; Qiao, L.; Guan, J.; Xu, H.; Wang, X.; Hu, P.; Du, H.; Li, S.; Zhou, X.; et al. Novel Design Concepts of Efficient Mg-Ion Electrolytes toward High-Performance Magnesium-Selenium and Magnesium-Sulfur Batteries. *Adv. Energy Mater.* **2017**, *7*, 1602055. [[CrossRef](#)]
94. Mohtadi, R.; Matsui, M.; Arthur, T.S.; Hwang, S.J. Magnesium borohydride: From hydrogen storage to magnesium battery. *Angew. Chem. Int. Ed. Engl.* **2012**, *51*, 9780–9783. [[CrossRef](#)] [[PubMed](#)]
95. Xu, H.; Zhang, Z.; Cui, Z.; Du, A.; Lu, C.; Dong, S.; Ma, J.; Zhou, X.; Cui, G. Strong anion receptor-assisted boron-based Mg electrolyte with wide electrochemical window and non-nucleophilic characteristic. *Electrochim. Commun.* **2017**, *83*, 72–76. [[CrossRef](#)]
96. Zhao, X.; Yang, Y.; NuLi, Y.; Li, D.; Wang, Y.; Xiang, X. A new class of electrolytes based on magnesium bis(diisopropyl)amide for magnesium-sulfur batteries. *Chem. Commun.* **2019**, *55*, 6086–6089. [[CrossRef](#)] [[PubMed](#)]
97. Fan, H.; Zheng, Z.; Zhao, L.; Li, W.; Wang, J.; Dai, M.; Zhao, Y.; Xiao, J.; Wang, G.; Ding, X.; et al. Extending Cycle Life of Mg/S Battery by Activation of Mg Anode/Electrolyte Interface through an LiCl-Assisted $MgCl_2$ Solubilization Mechanism. *Adv. Funct. Mater.* **2020**, *30*, 1909370. [[CrossRef](#)]
98. Xu, Y.; Zhou, G.; Zhao, S.; Li, W.; Shi, F.; Li, J.; Feng, J.; Zhao, Y.; Wu, Y.; Guo, J.; et al. Improving a Mg/S Battery with YCl_3 Additive and Magnesium Polysulfide. *Adv. Sci.* **2019**, *6*, 1800981. [[CrossRef](#)]
99. Xue, L.; Li, Y.; Hu, A.; Zhou, M.; Chen, W.; Lei, T.; Yan, Y.; Huang, J.; Yang, C.; Wang, X.; et al. In Situ/Operando Raman Techniques in Lithium–Sulfur Batteries. *Small Struct.* **2022**, *3*, 2100170. [[CrossRef](#)]
100. Cuan, J.; Zhou, Y.; Zhou, T.; Ling, S.; Rui, K.; Guo, Z.; Liu, H.; Yu, X. Borohydride-Scaffolded Li/Na/Mg Fast Ionic Conductors for Promising Solid-State Electrolytes. *Adv. Mater.* **2019**, *31*, 2100170. [[CrossRef](#)]
101. Gao, T.; Hou, S.; Khue, H.; Wang, F.; Eidson, N.; Fan, X.; Han, F.; Luo, C.; Mao, M.; Li, X.; et al. Existence of Solid Electrolyte Interphase in Mg Batteries: Mg/S Chemistry as an Example. *ACS Appl. Mater. Inter.* **2018**, *10*, 14767–14776. [[CrossRef](#)]

Disclaimer/Publisher’s Note: The statements, opinions and data contained in all publications are solely those of the individual author(s) and contributor(s) and not of MDPI and/or the editor(s). MDPI and/or the editor(s) disclaim responsibility for any injury to people or property resulting from any ideas, methods, instructions or products referred to in the content.